Scientific African 18 (2022) e01419

Contents lists available at ScienceDirect

Scientific African

journal homepage: www.elsevier.com/locate/sciaf

The current state on usage of image mosaic algorithms

Bose Alex Lungisani, Caspar K. Lebekwe, Adamu Murtala Zungeru*, Abid Yahya

Department of Electrical, Computer and Telecommunications Engineering, Botswana International University of Science and Technology, Botswana

ARTICLE INFO

Article history:
Received 11 March 2022
Revised 6 September 2022
Accepted 25 October 2022

Editor: DR B Gyampoh

Keywords:
Frequency domain-based
Image mosaic
RANSAC
SIFT
Spatial domain-based
SURF

ABSTRACT

Intensive research has been done on image mosaic algorithms to improve the field of view through generated image mosaics. However, their usage varies from one field to another due to the challenges faced by image acquisition platforms. Moreover, the current imagery software packages used are computationally intensive to be used in real-time applications and are not economically affordable. Those that are open-source are limited due to the less amount of data used to test their mosaicing algorithms' performance. Therefore, detailed knowledge of appropriate mosaic algorithms suitable for real-time applications is needed to produce mosaics with less computational time and efficient feature point detection. A comprehensive survey that categorizes existing mosaic algorithms' adoption in various fields has not been done to the best of our knowledge. Firstly, we provide a comparison of the strengths, weaknesses, and uniqueness of the image mosaic algorithms across different fields, with emphasis on challenging issues, limitations, performance criteria, and mechanisms. Furthermore, this paper provides an up-to-date review of image mosaic algorithms in various domains as used in different fields. We further classify the usage of image mosaic algorithms based on the following domains: spatial, frequency, and combined spatial and frequency as used in agriculture, environmental monitoring, and medical imaging. In addition, an analysis was carried out on one of the promising algorithms based on improved SIFT with the aim of improvement. We then proposed an improved SIFT algorithm, which was then evaluated with an open-source algorithm and commercial software using structural similarity index measure (SSIM) and mosaicing computational times for mosaic accuracy and processing efficiency, respectively. Our approach demonstrated a significant improvement of more than 10% average on the mosaicing computational times for the five datasets used. Its mosaicing accuracy was found to be relatively within an acceptable range of above 90% averagely.

Introduction

An image mosaic is a composite image of a wide-angle scene [1] that represents a three-dimensional (3D) scene [2] formed from the transformation of overlapping images of the same or different cameras. A mosaic can be described

* Corresponding author.
E-mail address: zungerum@biust.ac.bw (A.M. Zungeru).

https://doi.org/10.1016/j.sciaf.2022.e01419

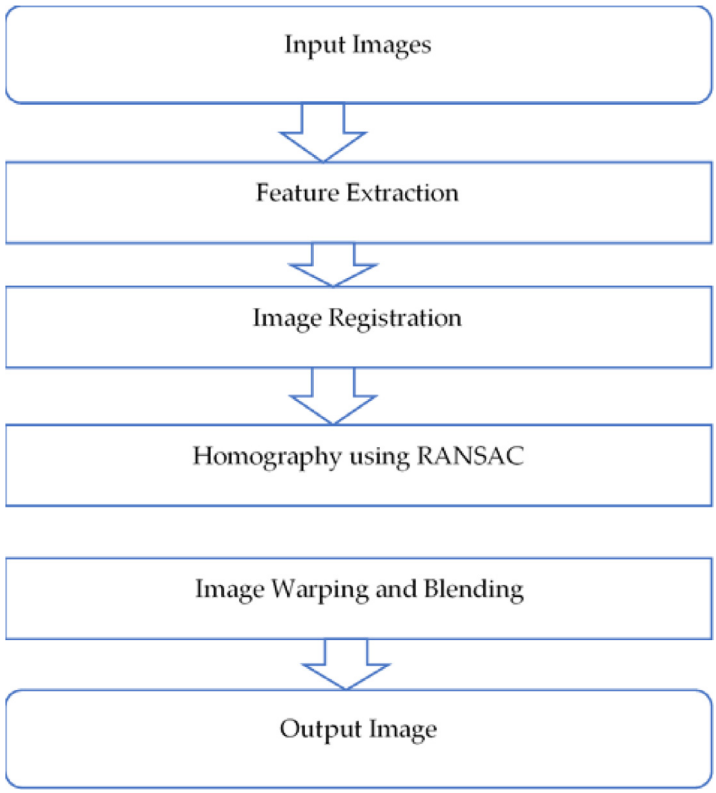

Fig. 1. Basic mosaicing flowchart [10,14].

as a process of automatically stitching frames of an object together to obtain a complete view of the object itself [3]. Image Mosaicing can be used to generate a panoramic image of high resolution from a combination of two or more images taken from the same scene [4]. Research activity in the field of image mosaics started in the early 1970s, and the interest continues even today to investigate the suitability of image mosaicing in different applications [5].

Generally, image mosaic techniques perform differently in different applications. For example, remote sensing in Unmanned Aerial Vehicle (UAV) photogrammetry is limited by flight height and focal length of the camera, resulting in smaller images [4,6]. Image mosaicing technology is being adopted to solve the problem of a single image being insufficient to represent the features of the target area under study [6]. Essential techniques of image mosaicing include image matching and image fusion.

Image matching: deals with finding similar features between images in a video or scene and considering them the same as a result [7].

Image fusion: gathers all the relevant information from several images to create a single image that depicts all the images involved [8]. Fig. 1 is an illustration of general steps required in image mosaicing across most applications, including videos or images from UAV or Remote-Controlled (RC) aircraft. Furthermore, the processes involved in creating an image mosaic can be summarized, as shown in Fig. 2. The process involves image registration, reprojection, stitching, and blending [1]. In computer vision, homography is mapping corresponding points from one image to another through transformation and generally through a 3×3 matrix.

Research on image mosaicing has been motivated by its wide range of applications [2,9], including UAV photogrammetry, medical imaging, astronomy, motion detection, resolution enhancement, land surveying, crop monitoring, etc. Several image mosaicing algorithms in the literature have previously been categorized according to image registration and image blending [2,10]. Image registration can be defined as a prerequisite for visible light and infrared image fusion [11]. Accuracy in image registration is a critical requirement for most applications of remote sensing images [12]. Image registration mosaicing algorithms can be classified into Spatial domain-based and Frequency domain-based [13]. Recently, mosaicing algorithms have been classified based on the extent of overlapping as demonstrated in Fig. 3.

Much research has been done on the review of mosaicing algorithms [2,4,15–21].

The research work contributions of this paper are as follows:

(1) A survey and comparison of existing image mosaic algorithms according to their strengths, weaknesses, and uniqueness, with emphasis on challenging issues, limitations, performance criteria, and mechanisms.

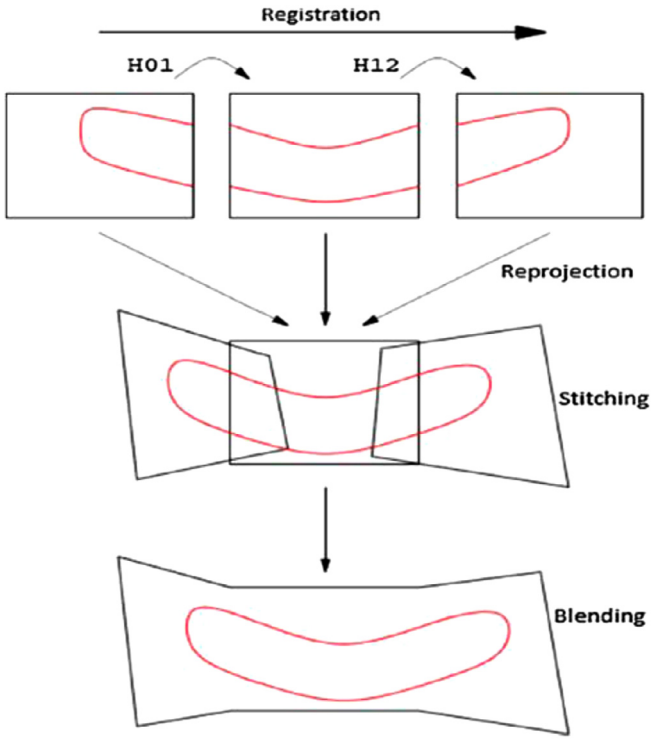

Fig. 2. Image mosaicing steps with homography matrices are denoted by H [2].

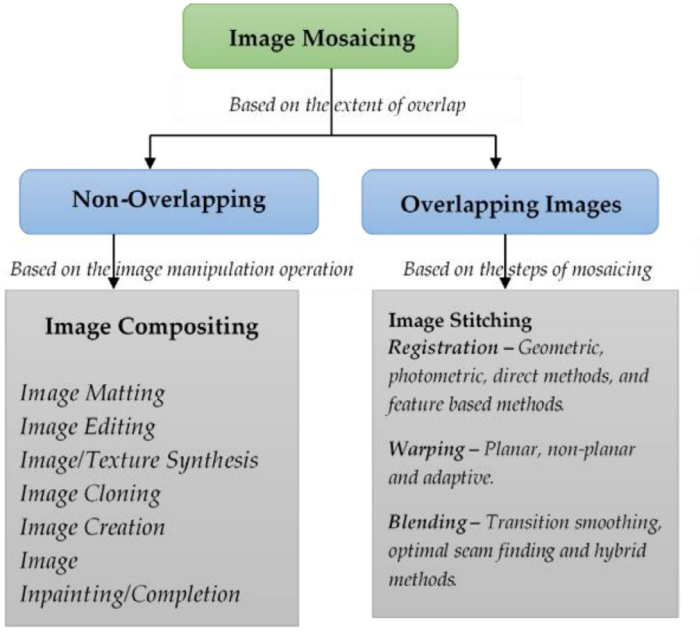

Fig. 3. Classification of image mosaicing algorithms based on the extent of overlap [10].

(2) Classification of image mosaicing algorithms' domains according to their usage in agriculture, environmental monitoring, and medical imaging. The domain image mosaicing algorithms were classified as frequency domain-based, spatial domain-based, and combined spatial and frequency domain-based.
(3) Analysis and simulation of the Improved SIFT algorithm [22] that utilizes adaptive contrast thresholding on the Difference of Gaussians (DOG) scale-space, traverse, and longitudinal overlapping to improve feature points detection efficiency, and matching accuracy, respectively with the aim of improvement in image mosaic accuracy and computational times of the algorithm.
(4) We proposed an improved SIFT algorithm, with an improvement of more than 10% average on the mosaicing computational times for the five datasets used, which was found to have mosaicing accuracy to be relatively within an acceptable range of above 90% averagely.
(5) An evaluation of two image mosaic algorithms that include the Improved SIFT algorithm [22], and commercial software [23] using structural similarity index (SSIM) and image mosaicing computational times as similarity measures. In addition, drawing up guidance on future research key factors to be considered in image mosaicing based on the researched literature.

The rest of the paper is organized as follows: Section 2 classifies related work according to strengths, uniqueness, and weakness of mosaicing algorithms. Section 3 discusses the different existing, commonly used image mosaicing algorithms' techniques. In Section 4, the various mosaicing algorithms applied to different fields are discussed. In Section 5, the classification of the algorithms as used in different fields is presented. An evaluation of the Improved SIFT [22] algorithm was done in Section 6. In Section 7 a proposed algorithm is outlined while in Section 8 an evaluation of two mosaicing algorithms that include the Improved SIFT algorithm [22] and commercial software is done, and finally, conclusions are drawn in Section 9.

Related work

Previous years' research on image mosaicing has focused on reviews of image mosaic algorithms and techniques in general. Previous surveys have been on the classification of image mosaic algorithms in image registration and image blending types of mosaicing algorithms. Tables 1 , 2 , and 3 provide a comparison of a few reviewed papers on image mosaic algorithms as used in the fields of agriculture, medical imaging, and environmental monitoring, respectively.

Image mosaicing techniques

In this section, image registration and blending techniques are discussed with emphasis on the image registration techniques. Several algorithms that perform image mosaicing are employed for each of these steps. Image registration is defined as the correlation of two or more images belonging to the same scene, where one image is considered a reference image [9,57]. The quality of image registration affects the generated mosaic [43]. Image blending is used for image morphing and consists of assigning overlapping regions with colors [65]. Furthermore, it has applications in image-based rendering and video compression [58]. Literature has demonstrated image registration techniques can be categorized into Frequency domain-based and Spatial domain-based algorithms.

Frequency domain-based algorithms

These techniques extract the similarities between two or more images through Fast Fourier transformation (FFT) by transforming images from spatial domain to frequency domain [59,58]. An image is represented based on its frequency content [4]. The computationally efficient algorithms used in this domain depend on finding the scale, rotation, and displacement in matching images [58]. However, these algorithms are more susceptible to noise, and the degree of overlap between matched images is less than 50%. Such methods include Phase correlation, Walsh transform, etc. Phase correlation can be described as a computationally efficient method that effectively estimates translations, rotations, and scaling from object and camera motions on video sequences [60]. It can be used to find translational coordinates used in image mosaicing [59].

Spatial domain-based algorithms

The literature suggests that these algorithms can be categorized as direct and feature-based methods. They rely on the distribution of features and low-level attributes of the images, such as pixels, intensity, etc., to do the image matching. These algorithms are computationally intensive compared to Frequency domain-based algorithms but are highly efficient in real-time applications [15]. Previous research also suggests that the algorithms can deal with illumination variations and overlapping of less than 50% between matched images.

Direct methods

These methods use pixel-to-pixel matching for image mosaicing. Direct methods generally compare corresponding pixels of several images [61]. Even though these methods are not invariant to the rotation and scaling of an image, they minimize the sum of absolute differences of the overlapping pixels [61]. In addition, they frequently use the following algorithms: *minimization on intensity, correlation methods, mutual information (MI)* for image mosaicing.

Table 1
Comparisons between the related works on image mosaic algorithms in agriculture.

Citation	Title of Paper	Year	Brief Description	Strengths	Weaknesses	Uniqueness
[22]	Rapid Mosaicking of Unmanned Aerial Vehicle (UAV) Images for Crop Growth Monitoring Using the SIFT Algorithm	2019	Integrates SIFT and RANSAC that uses adaptive contrast thresholding of DOG scale-space difference based on the UAV images contrast properties; thermal infrared, near infrared, and visible light.	Computational efficiency, image mosaicing validity at 0.9 using structural similarity index metric, can stitch together UAV images of low resolution.	A limited number of images for testing.	Quality and accuracy of image mosaicing kept intact through the integration of RANSAC to get rid of UAV images mismatched point pairs influence.
[24]	Aerial Monitoring of Rice Crop Variables using a UAV Robotic System.	2019	Crops automated monitoring through artificial neural networks and multi-variable regressions relationships on leaf nitrogen and biomass accumulation concentrations.	Nitrogen and biomass estimation capability through the crop's growth due to a mixture of green and yellow colors.	There is no system reliability on the crop reproduction stages.	Integration of machine learning and image processing algorithms in the analysis of multi-spectral UAV imagery to facilitate precision agriculture.
[26]	Image Mosaicing Using Multi-Modal Images for Generation of Tomato Growth State Map	2018	Generates mosaic by using the Information on distance to get rid of Background scenes and cultivation lanes at the back of the targeted area. Also uses infrared images to get rid of feature points correspondence problem.	Identification of ripe tomatoes through a greenhouse mosaiced map	Not fully automated, harvest times cannot be estimated	Used infrared images to generate an RGB mosaic
[27]	Fast and Robust Image Sequence Mosaicking of Nursery Plug Tray Images	2018	PC-SURF image mosaic algorithm to improve the performance of the sowing of the nursery tray.	The accuracy of point matching and image mosaicing was better than that of a standard SURF, Image mosaic speed almost similar to that of real-time rice sowing systems.	Image distortions and contrast variations not addressed by the study	Integration of phase correlation and SURF to locate regions overlapping by reducing the area to be processed.
[28]	Automatic Semantic Segmentation and Classification of Remote Sensing Data for Agriculture	2018	Automated semantic segmentation and improvement of feature matching accuracy through CNN	Classification and segmentation accuracy guaranteed	Lacked in computational performance	Use of convolutional neural networks in feature extraction
[29]	Remote Sensing Image Mosaic Technology based on SURF Algorithm in Agriculture	2018	Rapid image splicing through SURF and Levenberg-Marquardt (L-M) on UAV images from farmland.	Reduction in cumulative errors, Automated mosaicing an area surveyed.	Algorithm tested on a clean and calm environment	Concentration on better flight planning to get rid of the UAV image acquisition problem of UAV low altitude limitations.
[30]	Accurate ortho-mosaicked six-band multi-Spectral UAV images as affected by mission planning for precision agriculture proposes	2017	Definition of the right parameters for flight planning to be used in improving ortho-imagery accuracy in the detection of weeds in crop seedlings.	Improvement of image mosaicing spatial accuracy, the definition of the right UAV altitudes for high-resolution mosaics	Invariant elements ignored such as streetlamps.	Adoption of flight planning as a critical pre-requisite for the generation of high spectral and ultra-high spatial resolution mosaic
[32]	UAV Remote Sensing Image Mosaic and its Application in Agriculture	2016	Monitoring of crop growth, nutrient diagnosis, diseases, and pests using both multi-spectral and high-definition cameras for near-infrared and visible light UAV remote sensing image acquisitions.	The algorithm can be applied in a wide range of applications, useful in the acquisition of crop conditions information.	No quantitative evaluation is done	Image mosaic through SIFT, 3 $\times$ 3 meters cloth on radiometric calibration.

(*continued on next page*)

Table 1 (*continued*)

Citation	Title of Paper	Year	Brief Description	Strengths	Weaknesses	Uniqueness
[33]	Large Scale Image Mosaic Construction for Agricultural Applications Aperture Radar	2016	Mosaicing of UAV images captured at low altitudes and avoiding reliance on assumptions of depth variation negligibility and planar scene expectation on the computation of homography.	The method can handle large numbers of images and mosaics with high resolution and fewer misalignments.	Image sharpness not guaranteed	Images used for mosaicing took at low altitudes by a UAV conducting complicated motions.
[38]	Robust Spatial-Domain Based Super-Resolution Mosaicing of CubeSat Video Frames: Algorithm and Evaluation	2014	Integrates image mosaicing method and regeneration of super-resolution mosaic method based on the Huber prior information to resolve the super-resolution problem on CubeSat	Real-time applications efficiency	Not fully automated and illumination variations detection not guaranteed	Huber-based prior information is used to resolve multiple super-resolution problems.

Table 2
Comparisons between the related works on image mosaic algorithms in medical imaging.

Citation	Title of Paper	Year	Brief Description	Strengths	Weaknesses	Uniqueness
[31]	A Novel Hybrid Algorithm for Stitching of Spine Magnetic Resonance Images	2017	Stitching together of overlapping images through RANSAC and SIFT on cervical-thoracic lumbar (C-T-L) spine MRI images for diagnosis purposes.	Approach supportive for spinal cord examinations, and can be applied in other medical imaging modalities, robust to illumination variations.	Accuracy of the system not demonstrated	A hybrid algorithm that is robust to the input image sequences with outliers
[34]	Super-Resolved Retinal Image Mosaicing	2016	Automated high spatial retinal images mosaicing to increase FOV from images captured through low-cost cameras and low-quality images.	Clinical usability of the system	Lacked mosaic generation robustness	The exploitation of the motion of the eye done by the guidance of a patient.
[35]	Aggrandized Aspect Based Mosaicing Technique for Scientifically Stigmatized Airborne Synthetic	2016	Uses the theory Adaptive Random Sample in reducing the search area on SAR feature detection to improve image mosaic interpretation and computational performance	Practical, simple, mosaic enhancement, reduction in computational time as compared to other existing algorithms	Geometric distortion improvements and feature detection computational times improvement necessary	Reduction of The search area in image feature matching through the Kaze algorithm
[36]	A Novel Technique for Mosaicing of Medical Images	2014	It uses a three-step mosaicing algorithm based on a discrete cosine transform that aims at reducing alignment errors and intensity variations.	Generation of high quality, and seamless mosaics, efficacy in getting visually excellent image mosaics.	Commonly used evaluation metrics such as RMSE not utilized	Reprojection of images to a regular compositing surface.
[39]	Image Processing Aerial Thermal Images to Determine Water Stress on Crops	2013	Mosaicing of images using SIFT and RANSAC through the conversion of radiometric data to temperature data to discover water stress in temperature images for walnut fields.	Adoption of open-source software to achieve objectives that will usually be achieved by commercial software of high-cost licenses.	It cannot show differences in contrasts between water and non-water-stressed crops not automated, non-removal of hot spots in temperature heatmaps.	Conversion of images to a significant temperature image that was captured by a camera supported by a crop duster.

(*continued on next page*)

Table 2 (*continued*)

Citation	Title of Paper	Year	Brief Description	Strengths	Weaknesses	Uniqueness
[40]	Fast Mosaicing of Cystoscopic Images from Dense Correspondence: Combined Surf and TV-L1 Optical Flow Method	2013	Image registration based on the image texture.	Images of poor texture robustly registered, sub-pixel accuracy, and improved processing speed in mosaicing.	Image distortions not addressed	The use of both optical flow and a feature-based method to be adopted based on the image texture during image mosaicing.
[41]	An Approach for X-Ray Image Mosaicing Based on Speeded-Up Robust Features	2012	The method is based on SURF, RANSAC, and weighted average in stitching X-images of the spine.	Panoramic X-ray imaging application effectiveness.	Failure to deal with levels of noise in some instances	Combination of a weighted average method, SURF, and RANSAC in image mosaicing.
[42]	Graph-based construction of textured large field of view mosaics for bladder cancer diagnosis	2012	A robust image registration algorithm that overlays image pairs that are non-consecutive with less overlapping.	The algorithm can be adopted in many general image mosaicing problems.	High Computational times	Creation of cystoscopy mosaics from multiple and different overlapping sequences of less than 50% on non-consecutive images.
[43]	Endoscopic Video Mosaicing: Application to Surgery and Diagnostics	2012	Analysis of the feature tracking and extraction from soft tissue surgery mosaicing perspective resulting in conceptual model design.	A conceptual model for localized deformation capturing presented to assist surgeons in doing surgeries	Fewer experiments and dataset not explicitly described	Consideration of challenges such as patient movements, breathing, etc. in image registration and feature tracking
[46]	Image Mosaicing for Evaluation of MRI Brain Tissue Abnormalities Segmentation Study	2011	Image mosaicing approach used in segmentation study on MRI brain abnormalities	Evaluation tool for brain tissue abnormalities segmentation	Fundamental techniques in image mosaicing not incorporated on the system	Use of image mosaicing as an evaluation tool in image segmentation
[47]	*In Vivo* Micro-Image Mosaicing	2011	An efficient pairwise image mosaicing algorithm with the possibility of being deployed in real-time with the use of probabilistic robotics in addressing global alignment and deformation of scenes.	It can be implemented in real-time, cumulative errors are dealt with.	No potential clinical effects of improving treatment and diagnosis.	All image deformations are shaped and rectified for in a solitary non-iterative optimization problem
[48]	Mosaicing of Optical Microscope Imagery Based on Visual Information	2011	Image mosaicing through local registration and the exploitation of visible information only	Effective in image mosaicing	Not applied to images of color	Suitability for working online together with non-motorized microscopes.
[49]	Fast construction of Panoramic images for cystoscopic exploration	2010	Consecutive image pairs linked by geometric transformations with a fast cross-correlation based initialization of translation parameters.	Mosaic construction takes less time	Not distortion-free	Cross-correlation translation parameters from image pairs for a fast start-up.
[50]	Mosaicing of Microscope Images based on SURF	2009	Image registration and feature matching through the use of an improved SURF algorithm in image matching speed	Accuracy on microscopy images with blob-like and repeating structures, image matching speed guaranteed, illumination, and color variations elimination.	Not fully automated	A division of descriptor windows in feature matching to increase the image matching speed.

(*continued on next page*)

Table 2 (*continued*)

Citation	Title of Paper	Year	Brief Description	Strengths	Weaknesses	Uniqueness
[51]	Mosaicing of Bladder Endoscopic Image Sequences: Distortion Calibration and Registration Algorithm	2008	Deploys a combination of mutual information and stochastic gradient optimization in registering consecutive images. Adjustment of local transformation matrices to get rid image distortions in the endoscopic analysis.	Rectification of endoscopic image distortions, mosaiced image visible aspect improvements, reasonable mosaiced images regarding bladders diagnosis.	Computational times and image registration accuracy not addressed	Image registration through a similarity metric on mutual information and stochastic gradient optimization
[52]	Automatic seamless mosaicing of microscopic images: enhancing the appearance with colour degradation compensation and wavelet-based blending	2008	Uses multiscale wavelet analysis for feature point extraction, feature points-based image matching, adjustments of color variations and degradation adjustments, and image blending	High performance on image sequences stained distinctively, effectiveness on degraded images, and those with color variations.	No comparison with other legacy systems	Deployment of the Gaussian-like model to improve the image mosaic differences in colors and optical degradation compensation
[54]	Deformable Image Mosaicing for Optical Biopsy	2007	Deploys an integration of distorted surface models that deal with image registration errors and local scene distortions.	Deals with image registration errors and scene distortions	Camera rotations not taken into consideration	Inclusion of non-rigid image transformations
[56]	Inverse image alignment method for image mosaicing and video stabilization in fundus indocyanine green angiography under confocal scanning laser ophthalmoscope	2003	Uses larger FOV employing diagnosis without resolution loss using an efficient image registration process. It is applied to blood vessel angiography using a confocal scanning laser ophthalmoscope.	A competent registration process	Effectiveness of the algorithm changes in the content of compared images cannot be guaranteed	Image registration through Sum of Squared Difference (SSD) minimization from inverse compositional image alignment
[57]	A Feature-Based Technique for Joint, Linear Estimation of Higher-Order Image-to Mosaic Transformations: Mosaicing the Curved Human Retina	2002	Image mosaics generated from many poor, uncalibrated views of the human retina by improving the previous algorithms on the same field of human retina analysis.	Accurate, more straightforward, offers more comprehensive coverage.	Algorithm tested on grayscale images only	Linear, feature-based, non-iterative method for jointly estimating consistent transformations of all images onto the mosaic anchor image

Minimization of Intensity: The most commonly used algorithm in the literature for reducing errors through intensity is the Marquardt-Levenberg minimization algorithm [62]. Minimization of intensity algorithms is applied during image transformations to correct the transformation matrix in image mosaicing.

Correlation methods: These methods are accurate and fastest when applied to image matching [63]. Examples include normalized cross-correlation (NCC), a similarity measure known for its simplicity, contrast, and brightness invariance [63].

Mutual Information (MI): This method emphasizes information theoretic concepts and can also be viewed as a statistical dependency measure between compared images using the histogram of the images [64].

Feature-based methods

Image registration uses the extraction of characteristic features [19], such as lines, segment points, curves, corners, etc., used for image matching. They are based on two-dimensional (2D) primitives [65] extraction and matching on overlapped images. The bottleneck of these methods is that they are computationally intensive [19]. However, they can deal with objects and camera motions such as zooming, rotation, etc. Feature-Based methods usually use the following algorithms:

Harris corner detection: The literature suggests that most feature-domain-based algorithms have been built from the Harris corner detection algorithm. Therefore, many algorithms in the literature have been proposed to improve upon the Harris corner detector. This algorithm is also known for its invariance in rotations, illumination, noise, and accuracy in the field of image processing [65,66].

Table 3
Comparisons between the related works on image mosaic algorithms in environmental monitoring.

Citation	Title of Paper	Year	Brief Description	Strengths	Weaknesses	Uniqueness
[25]	Underwater Video Mosaicing Using Topology and Super Pixel-Based Pairwise Stitching	2018	Mosaiced images of coral reefs acquired using hand-held cameras by scuba divers.	Better image mosaic quality as compared to the state-of-the-art methods	Lacked enough features for accurate mosaicing	Removal of loops and poor-quality image sections from the camera trajectory estimations, parallax-affected and parallax-unaffected image sections are stitched differently
[37]	Parallax Effect Free Mosaicing of Underwater Video Sequence Based on Texture Features	2014	Minimizes the underwater imagery parallax effects through the adoption of an efficient local alignment strategy after the global image registration process.	Reduce parallax effects on underwater generated mosaics	High computational times	Feature matching is done on texture features using CS-LBP.
[44]	A Novel Blending Technique for Underwater Gigamosaicing	2012	Image preprocessing, enhancements, and image blending to improve the quality of the visual aspects of the generated photomosaic	High-quality of the massive final mosaics of more than 5GB.	A problem of sharpening of consecutive images from distinct altitudes more especially on images of more imperfect qualities.	Solutions and strategies to tackling large underwater mosaicing described and applied.
[55]	An efficient method for geo-referenced video mosaicing for environmental monitoring	2005	Combines two distinct data sources to get seamless geo-referenced stitched image without global registration complexity.	Efficient in vital environmental operations	Errors in image transformations	Image mosaic achieved through a two-track method that combined two distinct data sources.

Scale Invariant Feature Transform (SIFT): This is a widely used algorithm in image mosaicing, 3D modeling, and robotic mapping, and it is invariant to rotation and scaling. The SIFT algorithm detects and describes local features in images [67] by extracting vital points of an object as a feature description of the object itself. It is a widely used detector [68].

Speeded Up Robust Features (SURF): The algorithm has proved to be robust and fast in image comparison, local, and similarity invariant representation [69–71]. Although it shares similar robustness with the SIFT algorithm, SURF is known to be faster [70]. The algorithm is based on feature detection and description. The enabling factor for SURF adoption in object tracking and recognition applications is its speed in computing operators through box-type convolution filters [69,71].

Features from Accelerated Segment Test (FAST): [72] defines a point of interest as a pixel in an image with a well-defined location that can be robustly detected. They are ideally repeatable between different images due to their higher local information content aspect [73]. Therefore, the FAST algorithm's main target is identifying these interest points in an image [74]. It was developed mainly for SLAM applications, where there are fewer computational resources [75,76].

Image mosaicing algorithms usage

Research has shown that the usage of image mosaicing algorithms is motivated by the improvement of the field-of-view of video images to achieve high-resolution mosaics with less noise, distortion, and blurring across different fields. Therefore, in this section, image mosaic algorithms are discussed based on the field of application. This research classified image mosaic algorithms according to agriculture, medical imaging, and environmental monitoring usage as shown in Section 2 on Tables 1–3.

Agriculture

The usage of image mosaic algorithms in agriculture has been widely adopted, especially with UAV images. This study has found that Spatial domain-based mosaic algorithms are highly used in agricultural applications, as shown in the reviewed literature.

A rapid image mosaic algorithm based on an improved SIFT algorithm was adopted in [22] to improve UAV images' mosaic effectiveness and efficiency in monitoring crop growth. This method adaptively sets a contrast-based threshold on the Gaussian (DOG) scale-space difference on UAV crops images contrasts. Hence, improving UAV image mosaic efficiency. Furthermore, RANSAC was inherited for quality assurance and accuracy of the generated mosaic. Experimental tests for

monitoring crop growth were done on thermal infrared, visible, and near-infrared UAV images. A dataset from UAV images of wheat and rice growth monitoring was used to carry out the tests. To evaluate the proposed algorithm, the authors compared their method with the standard SIFT (SSIFT) and Photoscan commercial mosaicing software. The results illustrated a reduction in computational time by 30%. The results also suggested that the UAV image mosaic accuracy was improved by 2.2–6.8% as compared to the SSIFT algorithm. According to the study, the algorithm was an essential breakthrough in assisting researchers in monitoring crop monitoring. Nevertheless, the dataset of a maximum of 10 images for different image sequences used in the authors' research is not enough to measure the computational performance of the algorithm. A system that combines machine learning and image processing algorithms of SURF and Oriented FAST and robust BRIEF (ORB) feature extraction, FLANN (Fast Library for Approximate Nearest Neighbors), was adopted for matching images.

In contrast to other related works, the authors in [24] used RANSAC to create homography and image transformations to complete the image mosaicing algorithm. Furthermore, the algorithm was used to analyze the multi-spectral aerial imagery for rice crop monitoring through UAV by calculating eight vegetation indices of images throughout the rice growth to ripening, including leaf nitrogen concentration and biomass accumulation. Experimental results showed estimations of 80% and 78% correlations for both nitrogen and biomass, respectively. From the conclusions drawn by the authors, the research did not address the imagery problem. This improved mosaicing algorithm opted to adopt the machine learning algorithms instead. Hence, a high-resolution image mosaic needs to investigate the imagery for improving quality monitoring of rice crops.

A SURF image mosaicing algorithm [26] was proposed to generate a tomato growth state map for the cultivation lane consisting of rows of tomatoes to achieve automated harvesting and tomato management in a greenhouse with necessary production facilities. A single mosaic image was generated from a dataset of 70 images captured from the greenhouse. A visual inspection of the generated mosaic was used to detect ripe tomatoes. The single mosaic image was extracted using feature points from two corresponding overlapping images. Homography matrix computation was done on the feature points of corresponding pairs to generate a stable mosaic. Moreover, the authors considered repeatability and feature points' distinctiveness and assumed that images were captured on the planar surface as preconditions for generating the desired mosaic. In evaluating their proposed algorithm, authors used a criterion for a correspondence determined from the robot's moving distance as follows:

$$150 \text{ pixels} < x1 \times 2 < 170 \text{ pixels}$$
$$-6 \text{ pixels} < y1\ y2 < 6 \text{ pixels}$$

Correct correspondences were achieved on satisfying the conditions set above. Results proved that a Red, Green, and Red (RGB) mosaic could be obtained from infrared images through homography matrix computation. A total of 302 tomatoes were detected through the algorithm, of which 184 were ripe from the generated mosaic of 70 images.

Even though the authors achieved the primary objective of detecting the ripe tomatoes for harvesting, the automation in detecting and marking the tomatoes as either ripe or not ripe was not addressed. The estimation of harvest time for better tomatoes' management still needs to be addressed.

An integration of Phase Correlation and Speeded up Robust Features (PC-SURF) in image mosaicing to minimize the computational complexity through phase correlation before locating overlapping regions using SURF was introduced in [27]. RANSAC was used for image blending and registration. This implementation was faster as test results demonstrated that PC-SURF out-performed the standard SURF algorithm in image mosaic accuracy by 7.14%. The algorithm was almost three times faster than SURF with a reduction in RMSE for RGB channels blending (RMSEr, RMSEg, and RMSEb) by roughly 8.4%, 6.9%, and 6.6%, respectively. Registration RMSE also decreased by 3%, with the overall speed of the mosaicing algorithm meeting real-time implementation requirements at 6.63 s/tray compared to 7.2 s/tray. The authors achieved the objective given the number of matching accuracies, time consumption, image registration, and blending accuracy. However, there were no discussions on how to address limitations that arise because of image distortions and contrast variations when coming up with a high-resolution mosaic.

The computational costs, processing capacity, and storage load of the legacy feature domain-based algorithms were addressed through a method suggested by authors in [28]. Automated segmentation and classification of remote sensing data for agriculture were also proposed therein. The algorithm used is based on the Harris corner detector to extract features of the image and Random Sample Consensus (RANSAC) for image registration and blending as a preprocessing stage for semantic segmentation using a self-organizing map (SOM). The optimization of neuron coefficients of the SOM was done using the swarm optimization technique (PSO). The results in [28] illustrated that Deep Residual Networks is a successful model in the Remote Sensing (RS) classification of images. The overall accuracy of 85% or more on all major crops was achieved using Convolutional Neural Network (CNN). Moreover, the results also illustrated an improvement in image classification and segmentation accuracy as compared to existing algorithms. Better recall and precision rates were achieved as compared to Simple Vector Machine (SVM), Random Forest (RF), Neural Network (NN), and ENN classifiers. The authors' research work also addressed the overall accuracy of the method in the agricultural system. However, they did not investigate improving the feature extraction and matching the existing algorithms used in image mosaicing. Hence, the need arises to improve these algorithms in computational complexity, simplicity, and processing time.

To resolve the problem of low-altitude UAV remote sensing image splicing, a SURF-based image mosaic technique for rapid image splicing was introduced in [29]. Levenberg-Marquardt (L-M) was used to optimize the mosaicing algorithm to minimize the photographic attitude and terrain fluctuation cumulative error. A dataset of 150 UAV images was used

as experimental splicing objects to generate a farmland panoramic image with high-resolution as well as at a low cost. Furthermore, comparison and analysis of SURF and SIFT on feature points detection were made through experiments. It was found out that SURF feature matching speed is higher than SIFT while keeping a higher image registration accuracy. Better stitching results were achieved through the optimized strategy of L-M in achieving the panoramic mosaic of the surveyed area. From the authors' objectives' viewpoint, they have achieved better results than other algorithms, such as the standard SURF algorithm. However, the fact that the algorithm was tested in a clean and calm environment without some atmospheric turbulences show a need to investigate a spatial domain of different conditions and carry out the same experiments through the UAV survey.

Considering that ortho-mosaiced images depend mainly on flight height and overlap percentage for spatial quality, an algorithm that uses a multi-rotor UAV combined with a multispectral camera on the mosaicing workflow by defining flight parameters effects was suggested in [30]. This research was motivated by the need to generate accurate ortho-images used for ortho-mosaicing. UAV flights were carried out at a defined altitude range of 30, 40, 50, 60, 70, 80, and 90 m above ground level. Agisoft PhotoScan software was used to generate an ortho-mosaic for weed seedling monitoring on crops. Authors found out that a 7040% overlap with an altitude range of 60–90% is required to keep a spatial accuracy in bundle adjustment. The results of that study were prominent in the detection of weeds within the crops. Even though the authors seem to have deliberately selected a study site of invariant elements abundance, their evaluations and experiments focused only on the flight altitudes as a critical area for investigating spatial accuracy. The study ignored invariant elements such as streetlamps, sidewalks, and zebra crossings as per their site area description. There is also a need to apply image fusion techniques in improving the spatial resolution of the ortho-mosaic.

Apart from using the SIFT algorithm for image mosaicing authors in [32] used multi-spectral and high-definition cameras to capture near-infrared and visible light remote sensing images. The paper discussed the monitoring of diseases and pests, crop growth, and nutrient diagnosis. The results illustrate that UAV remote sensing is pivotal in acquiring agricultural condition information for making informed decisions. Even though the authors outlined the importance of image mosaicing to get high-resolution mosaics through UAV remote sensing, the paper lacks some information on optimizing the already existing SIFT algorithm to improve performance. The dataset is described qualitatively but lacks a quantitative description, which is crucial in evaluating any image mosaicing algorithm performance, as suggested in the literature.

Unlike other researchers the authors in [33] focused on a high-resolution image mosaicing algorithm of UAV images obtained at low altitudes with complex motions. The main objective was to minimize the inter-image homography computations based on the planar scene with UAV flying at a bit more significant altitude negligence of depth variations. The authors indicated that this algorithm could handle many images used to generate an image mosaic with reduced misalignment and improved resolution. Quantitative evaluation with baseline systems such as SIFT, and Structure from Motion (SfM) was done through the root mean squared reprojection error (RMSRE) for each ground plane (P) given in (1)

$$RMSRE(P) = \sqrt{\frac{1}{N}\sum_{i=1}^{N}\left\|T^i(P) - p_i\right\|^2}, \tag{1}$$

The dataset used was motivated by agricultural applications and the need to avoid costly joint optimizations that are well known with existing algorithms and commercialized software. Even though the authors improved the existing mosaicing algorithms, image mosaicing quality assurance attributes such as image sharpness and grounds composed of multiple planes were not addressed.

In their research work in [38], the researchers used the SIFT and RANSAC homography to correct anomalies such as brightness errors and lens aberration in images. The focus therein is motivated by the desire to revolutionize the agricultural industry by exploring sensor and data-driven technology to increase agricultural yields. The goal was to determine water stress levels by assessing the usability of aerial imagery of walnut fields in Stockton, California. VLFeat opensource code that uses the SIFT feature extraction was used for image mosaicing. Boundaries for each image were increased to account for expanded images before combining the images. The study used a simple center-weighting methodology as a blending method during the stitching process in (2) and (3). The output value of a pixel of a mosaiced image is given by:

$$C(x) = \frac{\sum_k w_k(x) I_k(x)}{\sum_k w_k(x)}, \tag{2}$$

where $I_k(x)$ and $w_k(x)$ is the value and weight of pixel x in image k.

The weight of pixel x in image k is given by:

$$W_k(x) = \left|\min_y \{\|y\| | I_k(x+y)\}\right|, \tag{3}$$

The introduced blending method has its weakness in responding to slight errors in misalignment of the generated mosaics. The authors proved that a solution based on opensource software in image processing aerial images of small scale is feasible. It was observed that a dataset of ten images was used to test this algorithm. That worked well for a single UAV parse without any corrections needed in image mosaicing. However, this dataset is not enough to make reasonable conclusions, given that most farmers do large-scale farming. The authors' work highlighted the higher costs of licenses for commercial software that can process large amounts of data and a need for cheap, robust, and reliable image mosaicing algorithms for crop monitoring.

Medical imaging

Previous works have shown that image mosaics have been used in medical imaging to assist medical practitioners in diagnosing diseases with a better field of view from the generated mosaics. This paper found out that both frequency domain-based and Spatial domain-based image mosaic algorithms have been widely used with images from medical scanners and microscopes.

A hybrid technique based on SIFT and RANSAC for image mosaicing of C-T-L (cervical-thoracic-lumbar) spine magnetic resonance (MRI) images was introduced [77]. The solution was introduced in support of spine diagnosis improvements and human anatomy in general. Experiments were done on C-T-L image samples of a single patient. The strengths of both SIFT and RANSAC were utilized together to assist with the mosaic of C-T-L spine images. According to their viewpoint, this was a success. However, the authors used a dataset of a single sample that is a bit limited in making conclusions that can be relied upon. The generated mosaic's resolution strength and accuracy were not demonstrated in the paper despite some numeric and comparisons with legacy algorithms or other authors' works.

To achieve a large field of view (FOV) by acquiring images of the retinal fundus is very difficult. Therefore, [34] proposed an automated image mosaicing algorithm that increased FOV from low-quality images and cameras. An evaluation of the algorithm showed that generated mosaiced retinal images had up to 30° FOV in ten (10) different 15° FOV views through the experiments. Three experts in the human study field analyzed a dataset of twenty-four (24) super-resolved mosaics for retinal imaging. The dataset was essential for the decision-making and analysis of fundus images of color in clinical usability. The results suggested a need for an optimization approach through the integration of mosaicing and super-resolution to improve the mosaic generation's robustness.

The authors in [35] suggested a discrete cosine transform (DCT) based image mosaicing algorithm for medical images implemented through image alignment, reprojection, and blending to generate a seamless mosaiced image of high resolution. The algorithm was applied to X-ray, CT, MRI, angiogram from Fluorescein angiography of retina images as the dataset for experiments. In evaluating the algorithm, values for the standard deviation, entropy, and edge-based contrast measure (EBCM), and blurring metric of both the sets of original and mosaiced images were calculated and compared. These quality assessment measures showed that there were insignificant variations between the original images and the mosaiced images. Hence, the algorithm was categorized as robust to variations in image illuminations and transformations. Therefore, the authors found out that the image mosaic algorithm generated high resolution, and seamless medical imaging mosaics. The use of the commonly used quantitative evaluation metrics in image mosaicing algorithms, such as RMSE, could have been vital to the study to validate the robustness and the efficacy of the proposed algorithm.

A method with a choice based on the image texture using SURF and total variation L1-norm (TV) optical flow to improve the computational time of traditional image registration algorithms and accuracy in bladder wall stitching was proposed in [39]. TV optical flow is known for its illumination variability and a healthy degree of texture. The pig bladder is considered the same as the human bladder and was instead used to carry out the experiments. High-resolution images were captured from an opened pig bladder. A resultant mosaic without color breaks and texture implored that the mosaic was of high quality. On average, it was found out that for 50 images, there were 0.5 pixels per frame as the error in image registration. Therefore, it was concluded that the proposed algorithm had an accuracy comparable to other traditional algorithms with a speedup factor of 8 compared to a sparse ground-cut algorithm. Its efficiency was verified with phantom data. Even though the authors recommend their algorithm for other medical or non-medical imaging applications, the study did not address the errors that arise due to image distortions and noise.

An approach to mosaiced X-ray imaging of spine prototyping utilizing SURF, RANSAC, homography matrix estimation, and a weighted average method for image mosaicing was proposed in [40]. The proposed algorithm was an improved SURF method that used manual thresholding for feature extraction that is edge and noise sensitive. MATLAB was used for this algorithm implementation with vertebra images of different sizes as inputs. The findings showed that the algorithm proposed was robust to the local variations of the overlapping regions and small disparities in image alignments. However, the method cannot be adopted where there are contrast variations in medical image applications. Moreover, the algorithm suffered from the noise before image stitching. In some instances, it was shown that the level of noise in some images led to them not being considered consecutive images. At the same time, they were neighbors according to the original video sequences.

In improving of the textured field of view through large mosaics on the diagnosis of bladder cancer, authors in [77] proposed a graph-based mosaic construction. The method's other uniqueness is that it superimposed non-consecutive images of less than 50% overlap. Generated mosaics are highly enhanced on contrast resolution through non-linear optimization. A dataset of three pig bladders was used in the experiments.

The 10th image from the video sequences was extracted to avoid the accumulation of errors through globally targeted mosaicing errors. The authors proved that mosaics could be generated from multiple overlaps of video sequences where there are large geometric deformations through their algorithm. It is important to note that the study did not consider the computational time of the algorithm that can be improved significantly using some prior information using the Kalman filter or ignoring stagnant sections in terms of the movements on the trajectory of the trajectory cystoscope.

Limitations of the field of view from endoscopic cameras in minimally invasive surgery (MIS) were addressed by authors in [42] through a conceptual focus on tracking and extracting features adopted in soft-tissue operation mosaicing. The research was motivated by improving navigation through surgery by both new and experienced surgeons from challenges that

included deformed organs, patient movements, etc. To explore the soft-tissue video mosaicing problem, experimental tests were carried out using SIFT, SURF, FAST, Good features to track the pyramid approach (GFTT), and FAST pyramid approach. In their algorithm, the authors used the simple 128-dimensional SURF and 64-bit BRIEF descriptors. However, their article presented only the BRIEF descriptors analysis concept on local deformation in tissue capturing. Authors carried out fewer experiments that could validate their conceptual model on distinct textures and illumination variations. Furthermore, the data set used was not explicitly described even though the mosaiced images from the paper showed that there were some organs or tissues of interest used in the study.

In their research work, authors in [45] proposed an image mosaicing algorithm used as an evaluation tool for the segmentation study on Magnetic Resonance Imaging (MRI) brain abnormalities. The formation of fifty-seven (57) mosaicing images was from square, oval, and irregular shapes abnormalities. The Receiver Operating Characteristic (ROC) analysis was used to evaluate image mosaicing segmentation accuracies. The research found that image mosaicing used as an evaluation tool for diverse MRI brain medical data is of reasonable value and acceptable in addressing some of the challenges experienced with segmentation abnormalities results. Even though the proposed mosaicing method was used to measure image segmentation performance accuracy, it lacked some critical techniques in image mosaicing, such as feature matching, image transformation, etc.

As a way of outlining the importance of image mosaicing in medical imaging, especially the expansion of viewing fields and creating image maps for microanatomical structures, three algorithms were suggested [46]. These algorithms deal with miniature laser scanning microscopy (LSM) image sequences. The three algorithms proposed were based on efficient real-time pairwise image mosaicing, cumulative error eliminations, global and local alignments. The results demonstrated that compared to other existing image mosaicing algorithms in the literature, their algorithm corrected all distortions and transformed them into a single loop optimization problem. The algorithms RMSE improvement ranges were from 5 to 20% for global and local alignments, and a dataset of 93, 134, 80, and 20 images were used. However, the study did not try to determine what can be done further to improve the treatment and diagnosis when *in vivo* pathology from different imaging devices for precancerous or cancerous tissues.

To avoid over-reliance on motorized x-y stage offsets of optical microscopes that somehow take away the interaction between a microscope system and a researcher, the authors in [47] proposed an image mosaicing algorithm that exploited visuals' information local registration only. A real-time non-motorized approach that can work online through geometric and photometric consistencies was proposed. For evaluating the algorithm, real-time biological samples were captured in contrast phases using a stagnant optical microscope. Experimental results have shown the importance of choosing a suitable warping model for geometric registration improvement in image mosaicing. The efficacy of the algorithm has also been justified through the experiments. While it is evident from the study that the approach was able to deliver the expected results, it will also be of interest to evaluate the approach on color images and get a balanced analysis. Moreover, a more robust approach to selection criteria modeling is vital for drifts in errors emanating from the frame-to-frame approach adopted in the paper.

The study in [48] described an automatic, fast method based on cross-correlation to improve the cryoscopic analysis of bladder lesions' pathology through image mosaicing. Image registration was done through a geometric transformation. A dataset comprising of ten different image sequences of 150–1300 images was used. As a validating tool for the usability of this algorithm on real-time applications, image sequences were obtained during the clinical procedures. Sequences with exciting and challenging anatomical structures in the cystoscopic analysis were among the selected. Even though the authors managed to achieve a fast algorithm in building panoramic images of the inside of human bladders within minutes, computational times can still be improved through techniques predicting positions of previous images through information translation. Furthermore, the approach can further be improved to be able to deal with image distortions.

Authors in [49] proposed an image mosaicing algorithm of microscope system images based on SURF and RANSAC by improving the feature matching speed through a division of descriptor windows. Image smoothening in image blending was done using a weighted average method. Illumination changes and the density of objects was taken into consideration during the development process. The quality of the generated mosaic from the experiments and results was satisfactory, and the algorithm produced mosaics faster than existing algorithms on microscopy image sequences. The method can still be improved to automate the whole system to include image browsing, mosaicing for improving the diagnosis decision-making prospects on real-time medical application systems.

During image transformation, the authors in [50] introduced a direct mosaicing algorithm in using mutual information (MI) similarity metric and an optimization method based on a stochastic gradient. In their algorithm, the authors also implemented a simple method to deal with distortions that commonly affect endoscopic images through correlation. To improve the quality of the mosaiced image visually, adjustments were made to all matrices from the local transformation of images. For evaluation purposes, phantoms or pig bladder pictures were used to measure the image registration process limitations and the accuracy of the global mosaicing process that can cater for fiber scope displacements. The algorithm was tested on pig bladder pictures of two patients as a simulation for human bladders images in a firmly realistic environment. Even though the robustness and correctness of image distortions of the algorithm were achieved, the authors did not address some of the aspects that affect the efficacy of image mosaicing algorithms that include computational times, the accuracy of the image registration process. The dataset also did not pose any significant illumination variations that could explain how the algorithm responds to such data challenges.

The field of view limitation for magnified species motivated authors in [51] to consider an image mosaicing algorithm to improve color degradation and variations of specimens captured through microscopes through wavelet-based blending. Image transformations were done through 2D wavelet expressions. A frequency domain-based normalized correlation coefficient was used for image mosaicing. Noise influence on the detection of feature points was reduced through the edge correlation procedure. On evaluating their algorithm, a dataset of different stained images was used, including Hemoglobin-stained brain rat, stained human prostatitis tissue, etc. It was found out that the proposed algorithm responded well to poor quality images and efficient by making the mosaiced image more real with precise image registration. Additionally, it was found that SSD can be reduced by compensation, adjusting and degrading color in image registration while increasing the Cross-Correlation coefficient (CC). The study addressed some of the main challenges associated with image mosaicing, such as color variations, quality of the mosaiced image, distortions, etc. The results of this study lacked some comparisons with other algorithms on how well it responds to such challenges. Therefore, the level of efficiency and quality can be better evaluated through other algorithms.

Medical imaging applications, in most cases, work with transformations on non-rigid images. An image mosaicing algorithm that combines deformable surface models to recover the camera motion and the scene structure was proposed [53]. Manuna Kea CellVizio fibered confocal micro-endoscope was used for the experiments. The approach was tested on skin tissue. Averaging was used for image blending on overlapping pixels. Moreover, an optimization algorithm was used for modeling deformation with nine patches for each image. Cumulative errors from the registration process were corrected through global alignment to come up with a sharpened image mosaic from 93 images with a computational time of 73 s using an Intel Xeon 2.33 GHz processor machine. The algorithm was tested on several distinct data sets. According to the authors, image sequence alignment was a success together with non-rigid deformations corrections. However, the algorithm did not consider the camera rotations that might be important in other medical imaging applications. Furthermore, the paper did not address the implications of such an algorithm in assisting with optical biopsy diagnosis.

An application for fundus blood vessel angiography through confocal scanning laser ophthalmoscope (CSLO) based on SSD minimization between images during image registration to generate high-resolution mosaics used in diagnosis was introduced in [55]. The algorithm employed phase correlation technique to minimize illumination variations that might occur during image registration. In evaluating the Inverse Compositional image alignment method, 512 by 512 pixels of images of 256 grayscale levels from real indocyanine green angiography (ICGA) image sequences were used. The images used were images from more than 70 images of clinical patients. It was found out that SSD or NSSD stabilized earlier than the proposed algorithm. Moreover, the findings showed that the optimal use of statistical information of fundus images made the algorithm more reliable as compared to feature-based algorithms that depend on compositional image alignment. However, most of the conclusions were made from qualitative evaluation, even though there was an emphasis on statistical information. The study could not guarantee the effectiveness of the algorithm changes in the content of compared images.

In order to improve upon the previous algorithms in the literature on retinal image mosaicing, authors in [56] proposed a feature-based technique for joint, linear estimation of higher-order image-to-mosaic transformations using an image chosen as anchor image to be a reference point. The results for this image construction algorithm were analyzed based on around 20 images from 16 distinct eyes. The resulting panoramic images from three of the original 16 datasets were examined on resolution and numerically. Minor numerical error, alignment of images precisely, and close to no illumination variations were experienced from the simplification of the retinal mosaic. Therefore, the algorithm was proven to be helpful for the detection of retinal change and diagnosis of the choice of an anchor image from a variety of images. There is also a need to examine the algorithm of color retinal images as the authors in this paper used grayscale images for their experiments.

Environmental monitoring

Many image mosaic algorithms have been used in environmental monitoring applications, as shown in the literature. Such applications include underwater monitoring, land surveying, etc. It has been found out that spatial domain-based algorithms on UAV and robot images are used in environmental monitoring. Most of the algorithms have tried to address the challenges, such as parallax error, distortions, and blurring, affecting most image mosaicing algorithms, as discussed in the literature.

To achieve a high spatial resolution from more significant representations of UAV images, authors in [78] described the adoption of a simple image mosaicing method on scheduled flights for vegetation monitoring. A modification of the RANSAC algorithm for the automated homography estimation method was proposed. In homography estimation, one hundred and fifty matches between images instead of 50 with the lowest Euclidean distance were selected. For adjacent flight lines image feature matching, the SIFT algorithm from VLFeat open-source library was adopted to deliver the Euclidean distances and the feature matches. More than six sets of images for six distinct flights in a city and forest were used in evaluating their algorithm. MATLAB was used for the method implementation with a comparison done with Pix4DMapper Pro version 3.2.10 that uses SfM for ortho-mosaicing. The authors' results showed their algorithm was 6 min 48 s faster than the commercial software used. Moreover, geolocation errors for both X-axis and Y-axis had an RMSE of 0.5268 and 0.5598 meters compared to the commercial software with no color variations. However, it is worth noting that there were some substantial differences on the processing time and geolocation errors between the proposed algorithm and the commercial software. Therefore, emphasizing that it may have raised from homography estimations and inliers of the same pairs of images. Fur-

thermore, fewer than 200 images per UAV flight dataset is not enough to test the computational strength of an algorithm concerning processing time.

Research work in [25] presented an algorithm that minimizes distortions, parallax error, and object and effects due to camera motions that usually come with marine ecology imagery. To improve on these limitations, a two-step approach was proposed. Firstly, regions of low quality were removed based on the estimated trajectory of the camera. Secondly, parallax-affected, and parallax-unaffected were warped together differently through global transformations during image stitching to create panoramic views using SIFT and RANSAC. The method was tested in the Caribbean final region using underwater videos captured by a diver. Videos captured had between 2000 and 3500 frames with a resolution of 1080 $\times$ 1920 pixels reduced to 190 $\times$ 480 pixels for imagery processing.

Compared to previous algorithms on underwater imagery that use images from remote sensing and marine vehicles [79–81], their algorithm was robust to parallax error. Furthermore, the mosaic was found to be almost distortion-free with fewer misalignments. Due to the lack of enough features experienced in the author's research, there is need also to investigate frequency domain-based algorithms to improve image handling. Nonetheless, to improve computational time on detecting radar images, a search space reduction was achieved through an Adaptive Random Sample (ARS) theory.

An aggrandized aspect-based mosaicing approach that dealt with noise affecting airborne synthetic aperture radar (SAR) was proposed in [82]. Image interpretation was improved through the Kaze feature with a modified SIFT detection algorithm and M-SURF feature matching descriptor. Experimental results showed that the method was accurate and faster. Furthermore, it was found to be very active in matching images in real-time and feature recognition. The constructed image mosaics were free from noise that come with airborne imagery. Even though the overall computational time of the algorithm was improved, there is a need to improve the computational time for the feature detection process. Besides, there is also a need for geometric distortion improvements.

Minimization of image mosaics parallax error from video sequences captured from underwater was achieved through Centre Symmetric Local Binary Pattern (CS-LBP) and RANSAC using mutual offsets between images [36]. Global registration accuracy was improved with the adoption of adjustments in color distributions. The datasets included four video sequences suffering from parallax distortions on differing conditions of water that were captured 2 m from the water surface level. Evaluation metrics of precision and recall were used to compare the authors' algorithm with an existing auto-mosaicing method in the literature. It was found out that the precision and recalls of the procedure were high at 0.64 and 0.71, respectively, and a sound underwater-based mosaic was constructed. This can be applied to visual mappings, underwater navigation, and its applications, etc. Since parallax error negatively affects image stitching, there is also a need to improve computational times by detecting latent image overlapping through a match-it-all method.

The proposed solution on the research work in [37] was built from two key algorithms; an image construction algorithm using SIFT, Best Bins First (BBF), RANSAC, and a super-resolution reconstruction algorithm. However, to get rid of the super-resolution problem, known information through Huber prior was used. Datasets were from six UAV image sequences, and ten balloon images containing ten frames from high altitudes on a small satellite (CubeSat). Quantitative evaluation was done using several performance metrics. These included peak signal-to-noise ratio (PSNR), mean square error, cumulative probability blur detection (CPBD), etc. It was valid on CubeSat applications, as shown by high and low values on CPBD and PSNR. Blurring and noise from acquired images were addressed. Hence, the improvement in the quality of the mosaiced image. There is also a need to include more performance metrics that correlate with human visual systems used by most researchers in image mosaicing. Moreover, it will be ideal to fully automate the approach and test it on more extensive datasets of varying illuminations.

The approach in [43] was based on the quality improvement of a visual consistency of the final gigamosaicied image that covers a large area of kilometers underwater. These were achieved through enhancements in image pre-processing and blending. A combination of feature-based algorithms of SURF and SIFT was used for image matching purposes. For their experiments, there were varying image overlapping regions of 15–20%. To acquire images to be mosaiced, the Lucky Strike hydrothermal field was surveyed for three days using Victor-6000 ROV robot during boat cruising. Variations of contrasts due to differing acquisition altitudes have been compensated for through an adaptive contrast enhancement strategy. However, the algorithm did address color gigamosaicing. Also, there is a problem with sharpening consecutive images from distinct altitudes, especially on more poor-quality images.

In their research work [54], the authors focused on an efficient algorithm that excludes the computationally intensive global registration process in generating 2D geo-referenced seamless mosaic in near real-time is proposed. The approach was designed to eliminate the frame-to-frame error accumulation due to frame-to-frame image registration during mosaicing. The effectiveness is also achieved through a combination of two distinct data sources from a two-tracking method. Video images of 53 sampled video sequences of the natural forestry over The Nature Conservancy (TNC) testing site in Ohio and Brazil were used to carry out the image mosaicing experiments. The authors' experimental results maintain an accuracy achievement of 5–10 m of the resultant mosaics from video images at 2 m ground resolution. With a Pentium IV 2.0 GHz frequency IBM laptop, the most computationally intensive step for the proposed algorithm video alignment worked at 11.4 frames per second (fps) and 22.5 fps in a Xeon 2.4 GHz IBM dual-CPU Dell Desktop. Furthermore, it has been demonstrated that the effectiveness of the results was due to the deployment of the sensor motion information. In the study, some assumptions were made, such as assuming a constant range along the x-axis, which became problematic by creating errors at mosaic borders. The exclusion of the critical global registration from the geo-referenced aerial imagery to simplify the algorithm seems to have led to errors in image transformations.

Astronomy

Image mosaic algorithms have also been applied to astronomy, and literature has shown that the usage of such algorithms is not immune to challenges faced in other fields. Speeding up of the image registration process was achieved through a two-stage novel algorithm; the use of Linear Hough Transform (LHT) in [88] to determine angle motions, Normalized Cross-Correlation (NCC) for finding the displacement amount. Images were captured using the Canada-France-Hawaii Telescope. Therefore, to evaluate the accuracy, noise tolerance, and computation time, the algorithm was compared to the phase correlation (PC) method. Results have shown that astronomical images can be registered efficiently and effectively through the proposed approach. The use of angle motion and determination drastically reduce the search area. Hence, the algorithm outperforms the PC method on computational time, noise tolerance, and accuracy. An improvement of the algorithm on sequential registration of satellites and any other images of the camera in either zoom mode can also be made to test the algorithm.

General usage

A lot of algorithms do exist in the literature [17,56,70,83–87] that can be used in different applications and fields from observations during this study. However, due to the scope of this study, there was no in-depth research carried out based on this type of usage.

An Automatic Seamless Image Mosaicing method was proposed in [6]. This method creates a single large image (mosaic) by adopting a quadtree approach. The image was decomposed into sub-images to find the corresponding points in the sub-images, thereby reducing the search space in finding the correspondence between the pictures of interest. In their approach, texture features were extracted from the first quadrant of the first image and matched with all other four quadrants of the second image. Further division was done on the best-matched quadrants. In evaluating their method, the authors used the mean and standard deviation by testing the algorithm on different images and how it responded to the different pictures. Even though their results show a reduction in complexity to the order $2(\log_4(3n) - 1)$, where is the number of images, the assumption that the images to be mosaiced were orthonormal and distortion-free cannot be guaranteed in a practical environment. Furthermore, the method adopted by these authors did not consider contrast variations of images even though good results were obtained for brightness changes.

A Drift-Free Real-Time Sequential Mosaicing approach was proposed in [52]. This method significantly improves previous mosaicing techniques that require offline optimization or work in real-time but use the local alignment of nearby images and ultimately drift. The output mosaic was built using sequential Extend Kalman Filter Simultaneous and Localization Mapping (EKF SLAM). The collection was generated from triangular tiles attached to a backbone map over the unit sphere. Experimental results showed that all the drift from rotation estimation is minimized while allowing arbitrarily long sequences to be stitched into mosaics. It is also worth noting that the approach responded positively to the challenging natural scenes with jittery handheld camera movements, moving people, and changing illumination conditions. However, the procedure did not improve the quality of the mosaic generated in real-time but only concentrated on producing a real-time mosaic. Therefore, there is also a need to focus on the sharpening of the mosaic made in real-time.

The authors in [1] proposed a method to improve the drawbacks of SIFT and Redundant Keypoint Elimination (RKEM). The method was called Clustered RKEM (CRKEM) that reduced redundancy of extracted keypoints based on the keypoints distribution. The distance between features are proposed as redundancy index criterion. As compared to conventional methods such as SURF, SIFT-Improved Weighted Average, and ORB-Weighted Mean method, the authors' experiments demonstrated that there was superiority achieved from the proposed method in image mosaicing. Moreover, it found out that the proposed method improved the accuracy of image mosaicing. However, there is a need to validate the proposed method on other research areas such as image tracking.

Of recent, there was a survey on image mosaicing applied on UAVs [2]. Some of the recent publications that were reviewed include an image mosaicing for neonatal fundus images conference paper [3], 3D sequential image mosaicing for underwater navigation and mapping [4], parallel hashing-based matching for real-time aerial image mosaicing [5], and image mosaicking using improved auto-sorting algorithm and local difference-based harris features [6]

Classification of image mosaicing algorithms

The classification of the image algorithms surveyed in this research work determined data sets and image acquisition platforms as some attributes that are vital image mosaicing algorithms applications, as illustrated in Table 4 . Moreover, in Tables 4–6, the image mosaic algorithms were classified according to usage and domain from reviewed works. The findings demonstrated that Spatial domain-based algorithms had been highly adopted across the fields investigated. Our research work found out that spatial domain-based algorithms are highly used in agriculture, medical imaging, and environmental monitoring. It was also found that the spatial-based algorithms that are primarily adopted in image mosaicing usage on agriculture, medical imaging, and environmental monitoring are mostly feature based algorithms due to their strengths in dealing with illumination variations, matching accuracy, distortions, object, and camera motions. In Table 5, the usage of frequency domain-based algorithms in different fields is summarized. This includes the datasets and the image acquisition

Table 4
Spatial domain-based algorithms usage classification.

Citation	Mosaicing Algorithm	Field of Usage	Image acquisition platform	Main Objective(s)	Dataset
[22]	Improved SIFT	Agriculture	UAV	To improve UAV images mosaic effectiveness and efficiency in the monitoring of the growth of crops	Ten images of Rice and Wheat
[24]	Machine learning and image mosaicking processing algorithms of SURF and ORB feature extraction, FLANN Fast	Agriculture	UAV	Multispectral aerial imagery for rice crops monitoring	600 images of Rice
[26]	SURF Using Multi-Modal Images	Agriculture	Robots	To generate a tomato growth state map	70 images of Tomatoes
[28]	Harris corner detector	Agriculture	Satellite	To improve the computational costs, processing capacity and storage load of legacy feature-domain based algorithms	Landsat public dataset
[29]	SURF + Levenberg-Marquardt (L-M) for optimization of the mosaic	Agriculture	UAV	Resolve the problem of low-altitude UAV remote sensing image splicing	150 images of Rice
[30]	Agisoft PhotoScan Software similar to SIFT	Agriculture	UAV	To achieve a spatial quality improvement for detection of weeds	Unlimited number of Crops
[32]	SIFT	Agriculture	UAV	Monitoring of diseases and pests, crop growth and nutrient diagnosis	Rice and Corn
[33]	SfM software	Agriculture	UAV	Achieve high-resolution image mosaicing algorithm of UAV images obtained at low altitudes with complex motions	3500 and 540 images of UMN Horticulture Field Station and Corn respectively
[38]	VLFeat open-source code that uses SIFT	Agriculture	UAV	To determine water stress levels through the assessment of the usability of aerial imagery of walnut fields in Stockton, California	Ten images of Crops
[77]	SIFT+RANSAC	Medical Imaging	MRI scanner	Spine diagnosis improvements	Three images of C-T-L spine
[34]	Geometric and Photometric mosaicing	Medical Imaging	Mobile and low-cost camera	To develop an automated image mosaicing algorithm that increased FOV from low-quality images and cameras.	34 images of retinal fundus
[39]	SURF and total variation L1-norm (TV) optical flow	Medical Imaging	Cystoscope camera	To improve the computational time of traditional image registration algorithms and accuracy in bladder wall stitching that is known for its illumination variability and a substantial degree of texture	50 images of Pig bladder
[40]	Improved SURF + RANSAC + weighted average method	Medical Imaging	X-ray equipment of orthopaedic clinical	To develop a cost-effective X-ray medical image feature matching algorithm.	X-Ray Spine images
[77]	Combination of advantages of different state-of-art algorithms	Medical Imaging	Cystoscope camera	To robustly superimpose non-consecutive images of less than 50% overlap during image registration transformations	Every 10th image from a 25fps video was extracted from 3 pig bladders
[42]	Simple 128-dimensional SURF and 64-bit BRIEF descriptors	Medical Imaging	Not described	Understanding of feature extraction and tracking in image mosaicing	*in-vivo* soft tissue
[49]	Improved SURF, RANSAC, weighted average method	Medical Imaging	Olympus BX41 microscope system	To increase matching speed	Blur Red bone marrow

(*continued on next page*)

Table 4 (*continued*)

Citation	Mosaicing Algorithm	Field of Usage	Image acquisition platform	Main Objective(s)	Dataset
[50]	Mutual information	Medical Imaging	Endoscope	To develop a simple algorithm for correction of distortions from endoscope images	Pig bladder phantom sequences with concave internal walls on the *n*th image dynamic selection
[51]	The normalized correlation coefficient and modified Levenberg–Marquardt (MLM) method	Medical Imaging	Microscope	To improve color degradation and variations of specimens captured through microscopes through wavelet-based blending	Human prostatitis tissue tri-chromatically stained, rat brain stained by FoS immuno-histochemistry
[47]	Geometric and photometric, Direct linear transformation + RANSAC	Medical Imaging	Stagnant Optical Microscopy	To develop an algorithm that exploits information from visuals and local registration only to keep the researcher and microscopy interaction relationship	60 images of biological samples of altered bone tissue
[56]	Joint, Linear Estimation of Higher-Order Image-To Mosaic Transformations	Medical Imaging		To develop mosaicing algorithm for curved human retina that detects retinal change for diagnosis	20 retinal images from 16 distinct eyes
[78]	SIFT algorithm from VLFeat open-source library and Modification of RANSAC	Environmental monitoring	UAV	To develop a simple image mosaicing method on scheduled flights for vegetation monitoring	150 matches between images instead of 50 with the lowest Euclidean distance were selected in homography estimation
[25]	SIFT and RANSAC	Environmental Monitoring	Underwater vehicles	To reduce parallax error in marine ecology imagery through topology and super pixel-based pairwise	Videos captured had between 2000 and 3500 frames with a resolution of 1080×1920 pixels that was reduced to 190×480 pixels for imagery processing
[82]	Modified SURF (M-SURF)	Environmental Monitoring	Aircraft	To deal with noise affecting airborne synthetic aperture radar (SAR), improve computational time on detection of radar images, a reduction of the search space	Undefined
[36]	RANSAC using mutual information through Centre Symmetric Local Binary Pattern (CS-LBP) descriptor	Environmental Monitoring	monocular video camera	To minimize image mosaic parallax error from video sequences captured from underwater	Four video sequences suffering from parallax distortions on differing conditions of water that were obtained 2 meters from the water surface level
[37]	SIFT, Best Bins First (BBF), and RANSAC	Environmental Monitoring	UAV	To reduce the super-resolution problem	Ten frames from high altitudes on a small satellite (CubeSat
[43]	Integration of SURF and SIFT	Environmental Monitoring	Robot	To achieve quality improvement and visual consistency of the final gigamosaicied image that covers a large area of kilometers underwater	Lucky Strike hydrothermal field was surveyed for three days using Victor-6000 ROV robot

platforms used. Compared to spatial domain-based algorithms, the adoption of frequency domain-based algorithms in agriculture, medical imaging, and environmental monitoring was minimal. However, our study showed that most frequency domain-based algorithms are adopted in medical imaging.

Table 6 presents the usage of integration of Spatial domain-based, and Frequency domain-based algorithms as applied in agriculture, medical imaging, and astronomy. Research work carried out by this study on a few previous works showed that this type of integration is not common in the fields investigated. In Table 7, a usage frequency summary on the usage

Table 5
Frequency domain-based algorithms usage classification.

Citation	Mosaicing Algorithm	Domain	Field of Usage	Image acquisition platform	Main Objective(s)	Dataset
[45]	Pearson's correlation	Frequency	Medical Imaging	MRI scanner	To measure image segmentation performances accuracy	Brain Tissue of square, irregular, and oval shapes
[46]	template matching with normalized cross-correlation.	Frequency	Medical Imaging	Laser Scanning microscopy (LSM)	Deal with image registration cumulative errors	A dataset of 300, 93, 134, 80, and 20 human skin images
[48]	Cross-correlation using Fourier transform	Frequency	Medical Imaging	Cystoscopy camera	To propose a fast-mosaicing algorithm	Ten varying image sequences bladder lesions of 150-1300 images
[53]	Integration of several algorithms	Frequency	Medical Imaging	Manuna Kea CellVizio fibered confocal micro-endoscope	To achieve a non-rigid image transformation as opposed to rigid image transformations	Nine patches of skin tissue of 93 images
[55]	Phase Correlation and SSD	Frequency	Medical Imaging	Confocal scanning laser ophthalmoscope	To achieve SSD minimization between images during image registration to generate high-resolution mosaics for use in the diagnosis	More than 70 images of fundus blood vessel angiography from different patients
[54]	A two-track method with Kalman filtering	Frequency	Environmental Monitoring	Aerial Instrumentation	To exclude the computation-intensive global registration process in generating 2D geo-referenced seamless mosaic in near real-time	Video images of 53 sampled video sequences of the real forestry over The Nature Conservancy (TNC) testing site in Ohio and Brazil
[5]	Quad-tree Technique	Frequency	General	Space Shuttle	To reduce the search space in finding the correspondence between the pictures of interest	Natural, satellite, aerial and medical images
[52]	EKF SLAM (Extend Kalman Filter Simultaneous Localization And Mapping	Frequency	General	Low-cost hand-held Unibrain IEEE1394 camera	improvement on previous mosaicing techniques, which either require off-line optimization or which work in real-time but use the local alignment of nearby images and ultimately drift	Pedestrians walking around

Table 6
A combination of spatial-domain and frequency domain-based algorithms usage classification.

Citation	Mosaicing Algorithm	Field of Usage	Image acquisition platform	Main Objective(s)	Dataset
[27]	PC-SURF integration	Agriculture	A camera at a fixed interval of 1 s, 1.5 s and 2 s.	To develop an image mosaic algorithm that will attain the whole nursery tray sowing performance	Rice seedlings
[35]	Discrete cosine transforms (DCT) based phase Correlation, Direct and Feature-based	Medical Imaging	MRI. CT, X-Ray scanners	To achieve a seamless image mosaic generation in the presence of alignment errors and intensity discrepancies	CT, X-Ray, MRI, FA of retina images
[88]	Linear Hough Transform (LHT) and Normalized Cross-Correlation (NCC)	Astronomy	Canada-France-Hawaii Telescope	To speed-up the image registration process on astronomical images	30 synthetically created frames with displacement angle of 45° and the addition of Gaussian noise with zero mean and variance of 0.001.

Table 7
High-level summarization of the adoption of the algorithms.

Citation	Domain	Field of Usage	Usage Frequency
[22,24–26,28–30,33,34,36–40,42,43,45,47,49–51,56,77,78,82]	Spatial	Agriculture	9
		Medical Imaging	11
		Environmental Monitoring	6
31,34,35,37,38,39,40,41,43,44,46, 48,50,51,52,57,79,80,84]		Astronomy	0
		General	
[5,45,46,48,52–55]	Frequency	Agriculture	0
		Medical Imaging	5
		Environmental Monitoring	1
		Astronomy	0
		General	2
[27,35,88]	Spatial + Frequency	Agriculture	1
		Medical Imaging	1
		Environmental Monitoring	0
		Astronomy	1
		General	0

of reviewed image mosaic algorithms in different fields is presented. More than 70% of the reviewed algorithms are spatial domain-based applied to agriculture, medical imaging, and environmental monitoring. Besides, 42.3% of these spatial domain-based algorithms have been used in medical imaging, 36.6% in agriculture, and 23.1% in environmental monitoring applications. Less than 30% of overall usage is accounted for by frequency domain-based algorithms, mainly in medical imaging applications and integration of the two domains that account for 8.1% of overall usage.

Analysis of an image mosaic algorithm based on SIFT and RANSAC [22]

The algorithm optimizes contrast thresholding *Dc* that is setup dynamically in the DOG scale space in SIFT to improve accuracy and efficiency of UAV images in mosaicing. In addition, the algorithm was used for crop growth monitoring from UAV image mosaicing. Mis-matched feature point pairs were removed based on relative position relationships of the UAV images to improve accuracy of the algorithm. RANSAC was used to improve the matching accuracy of key points. The pseudocode in Section 7 describes the improvements made to the standard SIFF algorithm that uses RANSAC for transformation models. The simulations for this algorithm and our proposed solution were done in MATLAB R2020a.

The algorithm (Pseudocode 1)

Input: A Set of UAV Images I
Output: Mosaic Result U
1 Construct contrasts of image for set C = $\{C_i\}_{i=1}^{N}$ using (4);
2 Compute average contrast C*p* of image using (5);
3 **if** *I* are obtained by visible-light or near-infrared cameras **then**
4 Compute $\boldsymbol{D_{init}}$ using (6);
5 **end if**
6 **if** *I* are obtained by thermal infrared cameras **then**
7 Compute $\boldsymbol{D_{init}}$ using (7);
8 **end if**
9 Construct corresponding feature point sets F using $\boldsymbol{D_{init}}$;
10 Initialize **k1**= 1.1, **k2** = 1/1.1, $\boldsymbol{P_{min}}$, $\boldsymbol{P_{max}}$, *F;*
11 **repeat**
12 Step:
13 Update D_{new} using (8);
14 **until** *F* satisfies;
15 Update *F* by using (9) and (10);
16 Initialize P_{row}, P_{col};
17 **if** I_p and I_{p+1} have longitudinal overlap **then**
18 Update *F* using P_{row} using (11) and (12);
19 **end if**
20 **if** I_p and I_{p+1} have transverse overlap **then**
21 Update *F* using P_{col} using (13) and (14);
22 **end if**
23 *U* are acquired by *F*.

In this method a contrast *C* that expresses image details' differences is used to analyze the of image quality characteristics of the UAV images. The determination of the dynamic threshold took into consideration the different color-space of capturing devices to dynamically set the contrast threshold. The DOG scale-space contrast threshold D_c is a constant that is used to calculate the dynamic threshold for either thermal or visible images. This depends on the input image sequences. This is

denoted by D_{init} as the derived contrast threshold in the DOG scale-space. The retention of UAV image local features for a set of UAV image sequences, $I = \{I_p\}_{p=1}^{Q}$ is achieved by a 3 × 3 image block on the UAV image I_p being moved throughout the image to get the subdomain blocks, $Z = \{(I_p)_i\}_{i=1}^{N}$. Contrast for each subdomain Z_i is calculated and values of C are sorted in ascending order to determine image contrast median from the contrast $C = \{C_i\}_{i=1}^{N}$ sequence and image contrast C_p of UAV image I_p was calculate using (4) and (5).

$$C = \left[\frac{1}{N-1}\sum_{i=1}^{N}(x_i - \bar{x})^2\right]^{\frac{1}{2}}, \tag{4}$$

$$C_p = \frac{\sum_{i=1}^{N} C_i}{N}, \tag{5}$$

where $\bar{x}$ is the gray value of pixel points average of the derived subdomain. x_i is the gray value of pixel i in the subdomain. The N in (4) is the total number of pixels in a subdomain, which is nine (9) in this case for a 3 × 3 window. N in (5) represents the total number of subdomain contrasts within an image.

For feature points detection efficiency improvement, (6) is used reduce the matched feature points that are more than enough between two visible or near-infrared UAV images.

$$D_{init} = D_c \times \frac{C_p}{C_{me} - C_p}, \tag{6}$$

where C_{me} is the median of the image contrast sequence $\{C_i\}_{i=1}^{N}$, achieved through sorting the subdomains' contracts in ascending order.

For thermal infrared UAV images, the method ensures that there are enough feature points for matching and matching accuracy using (7).

$$D_{init} = D_c \times \frac{C_{me} - C_p}{C_p}, \tag{7}$$

To ensure that there are sufficient key points for matching transformation model computation, an appropriate contrast threshold D_{new} in the DOG scale-space is searched based on D_{init}. The maximum value P_{max} and minimum value P_{min} for the numbers of key points to be satisfied as constraints for feature matching and transformation through RANSAC are set. This also creates a reasonable range to guarantee accuracy in key point matching by unifying the number of feature points. The values of P_{max} and P_{min} are fixed and there is a need to adaptively set these values to respond to videos sequences of different structures effectively. k_1 is set at 1.1 and $k_2 = \frac{1}{k_1}$ and to interactively calculate the number of key points (F) between UAV images. Therefore, determining whether F meets the threshold criterion to get the final contrast threshold D_{new}in the DOG scale-space from D_{int} using (8).

$$D_{new} = \begin{cases} k_1 \times D_{init} & F > P_{max} \\ D_{init} & P_{min} < F < P_{max} \\ k_2 \times D_{init} & F < P_{min} \end{cases}, \tag{8}$$

Unused feature points were removed to improve the matching accuracy and improve computational times. In Section 1, Fig. 3 demonstrates that image overlapping is key in image matching. In the algorithm discussed [22], feature points removal of unused feature point pairs not in the overlap region are removed through traverse and longitudinal overlapping restrictions. Overlapping information details between images I_{p+1} and I_p, row number difference $\Delta\theta$ and column number difference $\Delta\varphi$ for each pair of matched key points are used to set up criterion used to delete the mismatched point pairs using (9) and (10)

$$H_{P+1} \times (1 - P_{row}) < |P_\theta - Q_\theta| < H_{P+1} \times P_{row}, \tag{9}$$

$$W_{P+1} \times (1 - P_{col}) < |P_\varphi - Q_\varphi| < W_{P+1} \times P_{col}, \tag{10}$$

where P_θ, Q_θ and P_φ, Q_φ details the row number and column number of two images I_p and I_{p+1} key points locations, respectively. The length and width of the image to be matched I_{p+1} are denoted by H_{P+1} and W_{P+1}, respectively. P_{row} is the overlap rate of two images in the longitudinal direction, and P_{col} is the overlap rate of the two images in the traverse direction.

Longitudinal overlap rate P_{row} for two consecutive images I_p and I_{p+1} eliminates mismatched feature point pairs using (11) and (12) as the constraints.

$$H_P \times P_{row} < P_\theta < H_P, \tag{11}$$

$$0 < Q_\theta < H_{P+1} \times P_{row} \tag{12}$$

Transverse overlap rate P_{col} of consecutive images I_p and I_{p+1} deletes mismatched feature point pairs using (13) and (14) as the constraints.

$$W_P \times P_{col} < P_\varphi < W_P, \tag{13}$$

$$0 < Q_\varphi < W_{P+1} \times P_{col}, \tag{14}$$

where H_P and W_P are the length and width of the image to be matched image I_p, respectively.

Proposed algorithm

According to literature, feature point detection efficiency and feature point matching accuracy are key attributes for a successful mosaicing process using SIFT algorithm. A successful feature point detection and matching depends on the strength of the contrast threshold. Therefore, a value set as the contrast threshold has to be adaptive to the image sequences being examined and mosaiced. Static thresholding cannot be relied upon on real-time applications as it compromises the mosaicing accuracy. Image sequences from different videos have different contrasts, structures and fall into different spectral band regions. Therefore, optimizing the dynamic threshold to be adaptive to image sequences to be mosaiced can offer better results [22].

Our proposed solution optimizes the adaptive threshold in [22] further by using histograms of image blocks instead of pixels and pixel values. Therefore, (4) and (5) were modified to further calculate the histograms to be used in calculating the contrast of blocks or windows of images that constitutes to the overall contrast of the image. According to the literature, an image histogram is less susceptible to illumination variations. Due to an increase in complexity by adding the histogram calculations to the algorithm in [22], by reducing (4) and (5) to one equation results in a good tradeoff between feature point detection efficiency and computational times. This is achieved by calculating the contrast per block instead of it being calculated from each pixel of the block. Therefore, iterating through blocks of the image instead of each pixel in a block of an image reduces the complexity our algorithm. An improvement to (4) and (5) is demonstrated in (15) as one equation.

$$C_p = \left[\frac{1}{N-1} \sum_{i=1}^{N} \left(h_i - \bar{h}\right)^2 \right]^{\frac{1}{2}}, \tag{15}$$

where C_p is the contrast of an image calculated from histogram values of blocks instead of pixel values of blocks like in (4). N is the total number of blocks in an image, i represents each block. h_i is the histogram value of a block and $\bar{h}$ is the average of the histogram values in an image.

The other structures of the algorithm in [22] remained the same. The algorithm was developed and simulated on MATLAB R2020a, and the results of the algorithm are in Section 8, Table 8. However, further improvements to the algorithm in [22] can be made in future. Image sequences have different characteristics ranging from quality, capturing device, captured video sequence field type, etc. Therefore, number of feature points in one image sequences for each image will most likely not be equal to that of a different image sequence. Therefore, there is need to adaptively set the appropriate range of the minimum (P_{min}) and maximum (P_{max}) number of feature point pairs to satisfy the registration requirements per image sequence. The P_{min} and P_{max} referenced and described in Section 6.

Evaluation of image mosaicing algorithms

In evaluating image mosaicing algorithms, several performance metrics proposed in the literature were used. The application of these performance metrics varies from one algorithm to another. Moreover, it has been realized that there is no single performance metric that can be used to compare all image mosaic algorithms. The plot ranking graphs of all algorithms reviewed were made difficult by the lack of a standard metric across surveyed works. Some of these metrics include Root Mean Square Error (RMSE), Mean Absolute Error (MAE), Normalized Difference Vegetation Index (NDVI), Cumulative Probability of Blur Detection (CPBD), Mean Square Error (MSE), Peak Signal-to-Noise Ratio, Singular Value Decomposition-based measure (SVD), Precision, and Recall. However, from our research work it has been found out that the most appropriate evaluation methods include the mosaicing time consumption (T) and structural similarity index (SSIM). These methods were used to evaluate the computational times efficiency and mosaicing accuracy, respectively in this research work.

SSIM measures the similarity of two static images from the perspectives of brightness, contrast, and structure [22]. Hence, an ideal evaluation tool for real-time applications

$$SSIM(x,y) = \frac{(2\mu_x\mu_y + C_1)(2\sigma_x\sigma_y + C_2)}{\left(\mu_x^2 + \mu_y^2 + C_1\right)\left(\sigma_x^2 + \sigma_y^2 + C_2\right)}, \tag{16}$$

Table 8 shows the results from the algorithms analyzed for a dataset of 60 UAV images classified as RGB, thermal and multispectral. The computational times and SSIM were recorded together with the sizes of images. The dataset used was from *senseFly* company website [23] and *Harvard Dataverse* [89]. Image sequences of different sizes in different fields were used. The results demonstrated that adaptive threshold adopted in [22] increases the accuracy of the resultant mosaic. The

Table 8
Image mosaicing results of UAV images in different fields.

Algorithm	Dataset	Spectral Band Region of Dataset Sequence	Frame Size	Field of Application	Number of Images	SSIM	Computational Time(s)
Agisoft Metashape (commercial software) [23]	1	RGB	680 × 420	Agriculture	60	0.8091	40.618944
VLFeat Open-source Software [90]	1	RGB	680 × 420	Agriculture	60	0.9462	36.284133
Improved SIFT Algorithm [22]	1	RGB	680 × 420	Agriculture	60	0.9391	34.415355
Proposed Algorithm	1	RGB	680 × 420	Agriculture	60	0.9100	32.3996
[91]	1	RGB	680 × 420	Agriculture	60	0.9381	33.85282
[92]	1	RGB	680 × 420	Agriculture	60	0.8928	35.29778
Agisoft Metashape (commercial software) [23]	2	RGB	720 × 480	Environmental Monitoring	60	0.9395	41.54213
VLFeat Open-source Software [90]	2	RGB	720 × 480	Environmental Monitoring	60	0.9780	38.663426
Improved SIFT Algorithm [22]	2	RGB	720 × 480	Environmental Monitoring	60	0.9796	36.84511
Proposed Algorithm	2	RGB	720 × 480	Environmental Monitoring	60	0.9661	36.4359
[91]	2	RGB	720 × 480	Environmental Monitoring	60	0.9819	37.38468
[92]	2	RGB	720 × 480	Environmental Monitoring	60	0.9752	39.06371
Agisoft Metashape (commercial software) [23]	3	Thermal	640 × 512	Agriculture	60	0.9021	39.231789
VLFeat Open-source Software [90]	3	Thermal	640 × 512	Agriculture	60	0.8862	32.817490
Improved SIFT Algorithm [22]	3	Thermal	640 × 512	Agriculture	60	0.9261	31.846246
Proposed Algorithm	3	Thermal	640 × 512	Agriculture	60	0.9028	30.247251
[91]	3	Thermal	640 × 512	Agriculture		0.9137	31.375429
[92]	3	Thermal	640 × 512	Agriculture		0.8966	31.008342
Agisoft Metashape (commercial software) [23]	4	RGB	520 × 380	Environmental Monitoring	60	0.9351	39.256173
VLFeat Open-source Software [90]	4	RGB	520 × 380	Environmental Monitoring	60	0.9207	37.000894
Improved SIFT Algorithm [22]	4	RGB	520 × 380	Environmental Monitoring	60	0.9366	34.562522
Proposed Algorithm	4	RGB	520 × 380	Environmental Monitoring	60	0.9422	29.719414
[91]	4	RGB	520 × 380	Environmental Monitoring	60	0.93542	29.92378
[92]	4	RGB	520 × 380	Environmental Monitoring	60	0.94875	38.62843
Agisoft Metashape (commercial software) [23]	5	Multispectral	690 × 510	Agriculture	60	0.8837	44.564581
VLFeat Open-source Software [90]	5	Multispectral	690 × 510	Agriculture	60	0.8911	39.645088
Improved SIFT Algorithm [22]	5	Multispectral	690 × 510	Agriculture	60	0.8989	42.985412
Proposed Algorithm	5	Multispectral	690 × 510	Agriculture	60	0.9007	35.644944
[91]	5	Multispectral	690 × 510	Agriculture	60	0.8667	43.985122
[92]	5	Multispectral	690 × 510	Agriculture	60	0.9198	41.986423

Agisoft algorithm has high computational times due to generation of the three-dimensional mosaic and point clouds used for georeferencing. However, the efficiency of the compared algorithms demonstrated an insignificant difference between the algorithms. Therefore, emphasizing the strengths of the evaluated algorithms.

Fig. 4 demonstrates the mosaicing accuracy for six evaluated algorithms on five different datasets of sixty image sequences each. The image sequences were of RGB, thermal and multispectral bands. The algorithms evaluated demonstrated a positive response to the mosaiced image accuracy. Each algorithm showing an overall average accuracy of almost 80% and above in five datasets used. The key point limit for the Agisoft Metashape software was set to 40,000 with a Tie Limit of

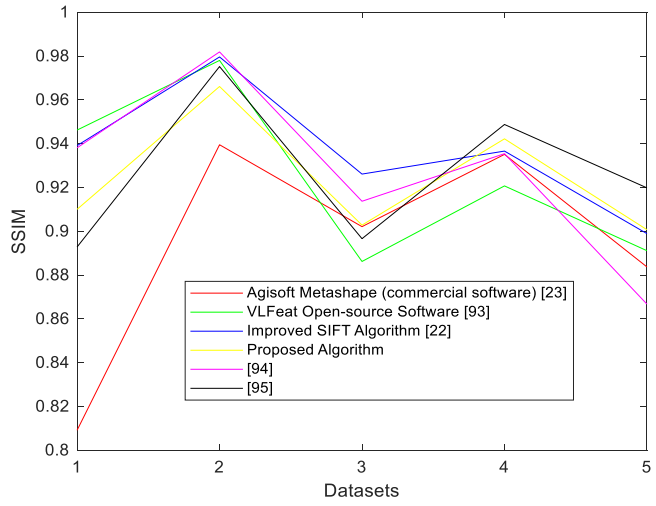

Fig. 4. A plot on mosaicing accuracy using SSIM for the six algorithms on five datasets.

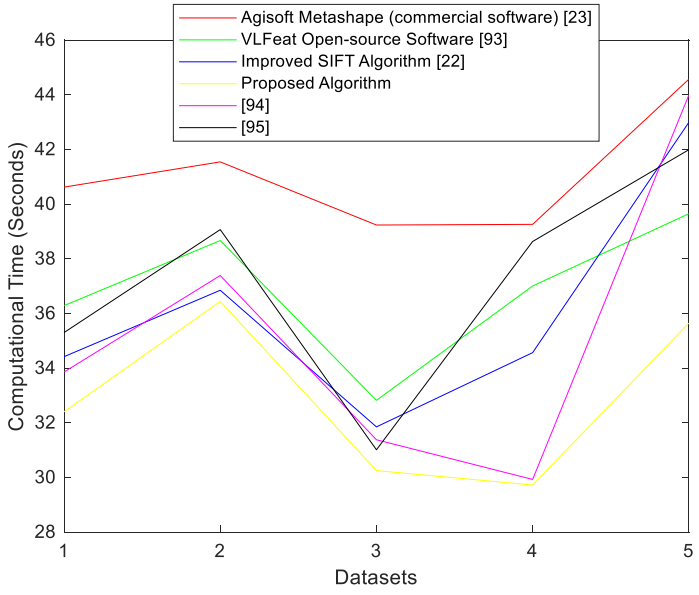

Fig. 5. A plot on mosaicing times for the six algorithms on five datasets.

4000 and accuracy set at high level. Our proposed algorithm's mosaicing accuracy is almost 90%. Therefore, an improvement done on the Improved SIFT algorithm has not significantly improved the accuracy but improved the computational times of mosaicing. This is illustrated by Fig. 5. Averagely, our proposed algorithm is on the top three in terms of mosaicing accuracy among the six evaluated algorithms.

In Fig. 5, the mosaicing times for the six algorithms are demonstrated. Our proposed algorithm has far better computational times. This can be attributed to the optimization of the adaptive contrast threshold. However, the Improved SIFT algorithm [22] demonstrated second best computational times than other evaluated algorithms. This was achieved through removal of mismatched point pairs. The commercial software has higher computational times related to the effort of producing ortho-mosaics used for georeferencing. An extra process that is not done by all other evaluated algorithms.

More interesting work on image mosaicing research works in different fields that were not part of this paper's scope can also be found in [93–122]. These include recent journal articles.

Conclusions and future direction

This research review aimed to bring together the literature on the current state of the usage of image mosaic algorithms. Tables 2 and 3 emphasize that Spatial domain-based algorithms have been adopted widely across different fields. The summary in Table 7 suggests that there is a partially balanced adoption of both frequency domain-based and spatial-based algorithms in the medical imaging fields. It is important to note that the algorithms adopted in agricultural and environmental monitoring fields are primarily based in the spatial domain. Our findings suggest that the Spatial domain-based algorithms that are adopted in most instances are feature-based. Furthermore, some integrated algorithms are based on Frequency domain-based and Spatial domain-based algorithms motivated by the utilization of each domain's strength. The accuracy of the mosaic depends on the contrast thresholding. The introduction of the adaptive dynamic contrast thresholding on the DOG scale space is key to obtaining an accurate mosaic through feature point detection efficiency. Each image in a video sequence may have its own level of contrast that may be different to the next image or another video sequence.

Key attributes in image mosaicing are the computational times, accuracy, and quality of the generated mosaic. The adoption of dynamic adaptive contrast threshold with SIFT algorithm offers a significant improvement in delivering real-time mosaics for precision agriculture. However, with further improvements as demonstrated by our proposed algorithm, better results can still be achieved by reducing the threshold complexity and accuracy of this algorithm. Therefore, the proposed algorithm may be a good start in the quest to produce a mosaic algorithm within reasonable computational times yet of high accuracy ranging from 90% and above measured through SSIM similarity measure from image sequences of different cameras and sensors in different fields. The number of feature point matches differ between images of different spectral bands regions. A mosaic algorithm should be able to process all types of images captured by different camera sensors. Parallelism with high-performance computer architectures is required to improve the overall mosaicing algorithms' performance.

Declaration of Competing Interest

The authors declare that they have no known competing financial interests or personal relationships that could have appeared to influence the work reported in this paper.

Acknowledgments

Appreciation goes to the Botswana International University of Science and Technology for providing various research platforms and resources used in this research. Also, much appreciation goes to the Department of Electrical, Computer, and Telecommunications for their motivation and support.

References

[1] R.M.S. Pir, Image mosaicing using MATLAB, Int. J. Eng. Dev. Res. 3 (2) (2015) 791–803.
[2] D. Ghosh, N. Kaabouch, A survey on image mosaicing techniques, J. Vis. Commun. Image Represent. 34 (2016) 1–11, doi:10.1016/j.jvcir.2015.10.014.
[3] R. Ialuna, G. Gagliano, D. Gravili, D. Tegolo, TECSIS: low-cost methodology to distinguish archaeological findings, Chem. Ecol. 22 (Supp1) (2006) 403–410, doi:10.1080/02757540600738500.
[4] S. Patil, A. Abhijeet, A review of image mosaicing methods, Int. J. Eng. Sci. 7 (4) (2016) 233–238, doi:10.5281/zenodo.5250.
[5] B. Ramesh, M. Ravishankar, Automatic seamless image mosaicing: an approach based on quad-tree technique, WCE World Congr. Eng. 1 (WCE) (2010) 687–691 2010.
[6] Y. Jia, Z. Su, Q. Zhang, Y. Zhang, Y. Gu, Z. Chen, Research on UAV remote sensing image mosaic method based on SIFT, Int. J. Signal Process. Image Process. Pattern Recognit. 8 (11) (2015) 365–374, doi:10.14257/ijsip.2015.8.11.33.
[7] N. Jayanthi, S. Indu, Comparison of image matching techniques, Int. J. Latest Trends Eng. Technol. 7 (3) (2016) 396–401, doi:10.21172/1.73.552.
[8] S. Masood, M. Sharif, M. Yasmin, M.A. Shahid, A. Rehman, Image fusion methods: a survey, J. Eng. Sci. Technol. Rev. 10 (6) (2017) 186–194, doi:10.25103/jestr.106.24.
[9] D. Vaghela, P.K. Naina, A Review of Image Mosaicing Techniques, Int. J. Adv. Res. Comput. Sci. Manage. Stud. 2 (3) (2014) 1–6.
[10] A. Pandey, U.C. Pati, Image mosaicing: a deeper insight, Image Vis. Comput. 89 (2019) 236–257, doi:10.1016/j.imavis.2019.07.002.
[11] C. Min, Y. Gu, Y. Li, F. Yang, Non-rigid infrared and visible image registration by enhanced affine transformation, Pattern Recognit. 106 (2020) 1–15, doi:10.1016/j.patcog.2020.107377.
[12] X. Li, N. Hui, H. Shen, Y. Fu, L. Zhang, A robust mosaicking procedure for high spatial resolution remote sensing images, ISPRS J. Photogramm. Remote Sens. 109 (2015) 108–125, doi:10.1016/j.isprsjprs.2015.09.009.
[13] J. Dadhore, V. Bisen, J.S. Dodiya, Image mosaic using phase correlation and Harris operator, Int. J. Emerg. Technol. Innov. Res. 4 (6) (2017) 220–225.
[14] T. Sato, et al., High-resolution video mosaicing for documents and photos by estimating camera motion, Comput. Imaging II 5299 (2004) 246, doi:10.1117/12.526510.
[15] M. Abdul-Rahim, Z.S. Yu, An in depth review paper on numerous image mosaicing approaches and techniques, Int. J. Eng. Manag. Res. 8 (02) (2018) 19–35, doi:10.31033/ijemr.v8i02.11607.
[16] L. Hathcock and R. MacNeille, "Mosaicking software: a comparison of various software suites," Geosystems Research Institute Report 5071, pp. 1-7, 2016. [Online]. Available: https://www.gri.msstate.edu/publications/docs/2016/03/15021Mosaic_Software_V5.pdf.
[17] H. Song, C. Yang, J. Zhang, W.C. Hoffmann, D. He, J.A. Thomasson, Comparison of mosaicking techniques for airborne images from consumer-grade cameras, J. Appl. Remote Sens. 10 (1) (2016) 16–30, doi:10.1117/1.jrs.10.016030.
[18] E. Adel, M. Elmogy, H. Elbakry, Image stitching based on feature extraction techniques: a survey, Int. J. Comput. Appl. 99 (6) (2014) 1–8, doi:10.5120/17374-7818.
[19] S. Ait-Aoudia, R. Mahiou, H. Djebli, E.H. Guerrout, Satellite and aerial image mosaicing - a comparative insight, in: Proceedings of the International Conference on Information Visualisation, 2012, pp. 652–657, doi:10.1109/IV.2012.113.
[20] X. Li, R. Feng, X. Guan, H. Shen, L. Zhang, Remote sensing image mosaicking: achievements and challenges, IEEE Geosci. Remote Sens. Mag. 7 (4) (2019) 8–22, doi:10.1109/MGRS.2019.2921780.
[21] S. Lafkih, Y. Zaz, Image mosaicing review: application on solar plant frames, in: Proceedings of the International Conference on Multimedia Computing and Systems, 2018, 2018, pp. 1–7, doi:10.1109/ICMCS.2018.8525865. May.

[22] J. Zhao, et al., Rapid mosaicking of unmanned aerial vehicle (UAV) images for crop growth monitoring using the SIFT algorithm, Remote Sens. 11 (10) (2019) 1–19, doi:10.3390/rs11101226.

[23] M. O'Sullivan, "AgEagle," Drones, sensors and software for automated aerial intelligence 2010. [Online]. Available: https://www.sensefly.com/education/datasets/?industries%5B%5D=2 (accessed Jan. 26, 2021).

[24] C. Devia, et al., Aerial monitoring of rice crop variables using an UAV robotic system, in: Proceedings of the 16th International Conference on Informatics in Control, Automation and Robotics, 2, ICINCO, 2019, pp. 97–103, doi:10.5220/0007909900970103. Icinco.

[25] Y. Li, C.J. Randall, R. van Woesik, E. Ribeiro, Underwater video mosaicing using topology and superpixel-based pairwise stitching, Expert Syst. Appl. 119 (2019) 171–183, doi:10.1016/j.eswa.2018.10.041.

[26] T. Fujinaga, S. Yasukawa, B. Li, K. Ishii, Image mosaicing using multi-modal images for generation of tomato growth state map, J. Robot. Mechatron. 30 (2) (2018) 187–197, doi:10.20965/jrm.2018.p0187.

[27] S.Y. Tan, X. Ma, L. Qi, Z.H. Li, Fast and robust image sequence mosaicking of nursery plug tray images, Int. J. Agric. Biol. Eng. 11 (3) (2018) 197–204, doi:10.25165/j.ijabe.20181103.2919.

[28] J.K. Jadhav, R.P. Singh, Automatic semantic segmentation and classification of remote sensing data for agriculture, Math. Model. Eng. 4 (2) (2018) 112–137, doi:10.21595/mme.2018.19840.

[29] W. Zhang, X. Li, J. Yu, M. Kumar, Y. Mao, Remote sensing image mosaic technology based on SURF algorithm in agriculture, EURASIP J. Image Video Process. 2018 (1) (2018) 1–9, doi:10.1186/s13640-018-0323-5.

[30] F.J. Mesas-Carrascosa, J. Torres-Sanchez, J.M. Pena, A. Garcia-Ferrer, L. Castillejo-Gomzalez, F.L. Granados, Generating UAV accurate ortho-mosaicked images using a six-band multispectral camera arrangement, in: Proceedings of the 2nd International Conference on Robotics and associated High--technologies and Equipment for Agriculture and Forestry, Madrid, Spain, 2014, pp. 1–10. May.

[31] M. Pornima, V. Patil, M.S. Chavan, A novel hybrid algorithm for stitching of spine magnetic resonance images, Int. J. Eng. Technol. 3 (3) (2017) 191–197 [Online]. Available: http://www.ijetjournal.org .

[32] Y. Jia, Z. Su, W. Shen, J. Yuan, Z. Xu, UAV remote sensing image mosaic and its application in agriculture, Int. J. Smart Home 10 (5) (2016) 159–170, doi:10.14257/ijsh.2016.10.5.15.

[33] Z. Li, V. Isler, Large scale image mosaic construction for agricultural applications technical report 16-002, IEEE Robot. Autom. Lett. 1 (1) (2016) 1–8.

[34] T. Kohler, A. Heinrich, A. Maier, J. Hornegger, R.P. Tornow, Super-resolved retinal image mosaicing, in: Proceedings of the International Symposium on Biomedical Imaging, 2016, pp. 1063–1067, doi:10.1109/ISBI.2016.7493449.

[35] A. Pandey, U.C. Pati, A novel technique for mosaicing of medical images, in: Proceedings of the 11th IEEE India Conference: Emerging Trends and Innovation in Technology, INDICON, 2015, pp. 1–5, doi:10.1109/INDICON.2014.7030465. 2014.

[36] S. Nagaraja, C.J. Prabhakar, P.P. Kumar, Parallax effect free mosaicing of underwater video sequence based on texture features, Signal Image Process. Int. J. 5 (5) (2014) 13–25, doi:10.5121/sipij.2014.5502.

[37] D. Ghosh, N. Kaabouch, R.A. Fevig, Robust spatial-domain based super-resolution mosaicing of CubeSat video frames: algorithm and evaluation, Comput. Inf. Sci. 7 (2) (2014) 68–81, doi:10.5539/cis.v7n2p68.

[38] P. Shah, "Image Processing Aerial Thermal Images to Determine Water Stress on Crops," 2013. [Online], Available: https://stacks.stanford.edu/file/druid:np318ty6250/Shah_Analysis_of_Canopy_Chemistry_in_Hyperspectral_Images.pdf.

[39] S. Ali, C. Daul, T. Weibel, W. Blondel, Fast mosaicing of cystoscopic images from dense correspondence: combined SURF and TV-L1 optical flow method, in: Proceedings of the IEEE International Conference on Image Processing, ICIP, 2013, pp. 1291–1295, doi:10.1109/ICIP.2013.6738266.

[40] H.M. Gong, J.H. Zhang, J.H. An, Z.Z. Zhao, W.W. Liu, An approach for X-ray image mosaicing based on Speeded-Up Robust Features, in: Proceedings of the International Conference on Wavelet Active Media Technology and Information Processing (ICWAMTIP), 2012, pp. 432–435, doi:10.1109/ICWAMTIP.2012.6413530.

[41] R. Prados, R. Garcia, N. Gracias, J. Escartín, L. Neumann, A novel blending technique for underwater gigamosaicing, IEEE J. Ocean. Eng. 37 (4) (2012) 626–644, doi:10.1109/JOE.2012.2204152.

[42] T. Weibel, C. Daul, D. Wolf, R. Rösch, F. Guillemin, Graph based construction of textured large field of view mosaics for bladder cancer diagnosis, Pattern Recognit. 45 (12) (2012) 4138–4150, doi:10.1016/j.patcog.2012.05.023.

[43] A.S. Vemuri, K. Liu, Y. Ho, H. Wu, Endoscopic video mosaicing : application to surgery and diagnostics, in: Proceedings of the Living Imaging, 2012, pp. 1–9.

[44] S. Shahhosseini, B. Rezaie, V. Emamian, Sequential image registration for astronomical images, in: Proceedings of the IEEE International Symposium on Multimedia, ISM 2012, 2012, pp. 314–317, doi:10.1109/ISM.2012.65.

[45] S. Ibrahim, N. Elaiza, A. Khalid, M. Manaf, Image mosaicing for evaluation of MRI brain tissue abnormalities segmentation study, Int. J. Biol. Biomed. Eng. 5 (4) (2011) 181–189.

[46] K.E. Loewke, et al., *In vivo* micro-image mosaicing, IEEE Trans. Biomed. Eng. 58 (1) (2011) 159–171.

[47] L. Carozza, A. Bevilacqua, F. Piccinini, Mosaicing of optical microscope imagery based on visual information, in: Proceedings of the Annual International Conference of the IEEE Engineering in Medicine and Biology Society, EMBS, 2011, pp. 6162–6165, doi:10.1109/IEMBS.2011.6091522.

[48] W. Rong, H. Chen, J. Liu, Y. Xu, R. Haeusler, Mosaicing of microscope images based on SURF, in: Proceedings of the 24th International Conference Image and Vision Computing New Zealand, IVCNZ, 2009, pp. 271–275, doi:10.1109/IVCNZ.2009.5378399.

[49] R. Miranda-Luna, C. Daul, W.C.P.M. Blondel, Y. Hernandez-Mier, D. Wolf, F. Guillemin, Mosaicing of bladder endoscopic image sequences: distortion calibration and registration algorithm, IEEE Trans. Biomed. Eng. 55 (2) (2008) 541–553, doi:10.1109/TBME.2007.903520.

[50] W.Y. Hsu, W.F.P. Poon, Y.N. Sun, Automatic seamless mosaicing of microscopic images: enhancing appearance with colour degradation compensation and wavelet-based blending, J. Microsc. 231 (3) (2008) 408–418, doi:10.1111/j.1365-2818.2008.02052.x.

[51] J. Civera, A.J. Davison, J.A. Magallón, J.M.M. Montiel, Drift-free real-time sequential mosaicing, Int. J. Comput. Vis. 81 (2) (2009) 128–137, doi:10.1007/s11263-008-0129-5.

[52] K. Loewke, D. Camarillo, K. Salisbury, S. Thrun, Deformable image mosaicing for optical biopsy, in: Proceedings of the IEEE International Conference on Computer Vision, 2007, pp. 3–10, doi:10.1109/ICCV.2007.4409111.

[53] Z. Zhu, E.M. Riseman, A.R. Hanson, H. Schultz, An efficient method for geo-referenced video mosaicing for environmental monitoring, Mach. Vis. Appl. 16 (4) (2005) 203–216, doi:10.1007/s00138-005-0173-x.

[54] Y. Zhou, H. Xue, M. Wan, Inverse image alignment method for image mosaicing and video stabilization in fundus indocyanine green angiography under confocal scanning laser ophthalmoscope, Comput. Med. Imaging Graph. 27 (6) (2003) 513–523, doi:10.1016/S0895-6111(03)00036-3.

[55] A. Can, C.V. Stewart, B. Roysam, H.L. Tanenbaum, A feature-based technique for joint, linear estimation of high-order image-to-mosaic transformations: mosaicing the curved human retina, IEEE Trans. Pattern Anal. Mach. Intell. 24 (3) (2002) 412–419, doi:10.1109/34.990145.

[56] S. Pandey, A. Potnis, M. Mishra, A detailed analysis on feature extraction techniques of panoramic image stitching algorithm, Int. J. Eng. Appl. Comput. Sci. 02 (05) (2017) 147–153, doi:10.24032/ijeacs/0205/01.

[57] D. Bhadane, K.N. Pawar, A review paper on various approaches for image mosaicing, Int. J. Eng. Manag. Res. 3 (4) (2013) 106–109 [Online]. Available http://www.ijemr.net/DOC/AReviewPaperOnVariousApproachesForImageMosaicing(193-195).pdf .

[58] T. Bouwmans, S. Javed, H. Zhang, Z. Lin, R. Otazo, On the applications of robust PCA in image and video processing, Proc. IEEE 106 (8) (2018) 1427–1457, doi:10.1109/JPROC.2018.2853589.

[59] Y. Keller, A. Averbuch, O. Miller, Robust phase correlation, in: Proceedings of the International Conference on Pattern Recognition, 2, 2004, pp. 740–743, doi:10.1109/ICPR.2004.1334365.

[60] S. Mistry, A. Patel, Image stitching using Harris feature detection, Int. Res. J. Eng. Technol. 03 (04) (2016) 1363–1369 [Online]. Available: www.irjet.net .

[61] V. DS, A.R. Bhat, S.P. M, V. Prakash, S. Kannan, Intensity based image mosaicing warp and bilinear interpolation, in: Proceedings of the 7th WSEAS International Conference of Applied Computer Science, 2007, pp. 111–116.
[62] M. Johar, S. Manjula, G. Namita, Image stitching using correlation method, Imp. J. Interdiscip. Res. 3 (2017) 282–290.
[63] S. Ghannam, A. Lynn, Cross correlation versus mutual information for image mosaicing, Int. J. Adv. Comput. Sci. Appl. 4 (11) (2013), doi:10.14569/ijacsa.2013.041113.
[64] E. Zagrouba, W. Barhoumi, S. Amri, An efficient image-mosaicing method based on multifeature matching, Mach. Vis. Appl. 20 (3) (2009) 139–162, doi:10.1007/s00138-007-0114-y.
[65] M. Brzeszcz, T.P. Breckon, Real-time construction and visualisation of drift-free video mosaics from unconstrained camera motion, J. Eng. 2015 (8) (2015) 229–240, doi:10.1049/joe.2015.0016.
[66] D. Capel, Image Mosaicing and Super-resolution, University of Oxford, 2001.
[67] S. Jayalaxmi, H. Ramachandran, Design of novel algorithm and architecture for feature based corner detection for image mosaicing, IOSR J. VLSI Signal Process. 4 (6) (2014) 12–24, doi:10.9790/4200-04631224.
[68] E. Karami, S. Prasad, M. Shehata, Image matching using SIFT, SURF, BRIEF and ORB: performance comparison for distorted images, in: Proceedings of the Newfoundland Electrical and Computer Engineering Conference, 2015, pp. 1–6. http://arxiv.org/abs/1710.02726. November 2015[Online]. Available:.
[69] E. Oyallon, J. Rabin, An analysis of the SURF method, Image Process. Line 5 (2004) (2015) 176–218, doi:10.5201/ipol.2015.69.
[70] H. Bay, A. Ess, T. Tuytelaars, L.V. Gool, Speeded-Up Robust Features (SURF), Comput. Vis. Image Underst. 110 (3) (2008) 346–359, doi:10.1016/j.cviu.2007.09.014.
[71] D. Viswanathan, "The evolving, Distributed, Non-Proprietary, On-Line Compendium of Computer Vision," 2011. [Online], Available: https://homepages.inf.ed.ac.uk/rbf/CVonline/Local_Copies/AV1011/AV1FeaturefromAcceleratedSegmentTest.pdf.
[72] H. Bay, T. Tuytelaars, L.V. Gool, SURF: Speeded Up Robust Features, Springer, 2006.
[73] D. Tyagi, "Introduction to FAST (Features from Accelerated Segment Test)," 2019. [Online], Available: https://medium.com/data-breach/introduction-to-fast-features-from-accelerated-segment-test-4ed33dde6d65.
[74] E. Rosten, R. Porter, T. Drummond, Faster and better: a machine learning approach to corner detection, IEEE Trans. Pattern Anal. Mach. Intell. 32 (1) (2010) 105–119, doi:10.1109/TPAMI.2008.275.
[75] D.G. Viswanathan, Features from accelerated segment test (FAST), in: Proceedings of the 10th Workshop on Image Analysis for Multimedia Interactive Services, 2009, pp. 6–8. http://homepages.inf.ed.ac.uk/rbf/CVonline/LOCAL_COPIES/AV1011/AV1FeaturefromAcceleratedSegmentTest.pdf. [Online]. Available:.
[76] M.D. Patidar, Automatic image mosaicing : an approach based on FFT, Int. J. Sci. Eng. Technol. 1 (1) (2011) 1–4.
[77] S. Ayushi, T.K. Taru, R. Kumar, Automated image mosaicing system with analysis over various image noise, Int. J. Comput. Sci. Appl. 6 (3) (2016) 13–24, doi:10.5121/ijcsa.2016.6202.
[78] M.K. Ramaiya, N. Tiwari, N. Hemrajani, P. Bhatnagar, Image mosaicing method by using sift and grid based, Int. J. Latest Technol. Eng. Manag. Appl. Sci. III (V) (2014) 332–337.
[79] D. Bhavya Lakshmi, N. Sathianandam, Aggrandized aspect based mosaicing technique for scientifically stigmatized airborne synthetic aperture radar, Int. J. Sci. Res. Sci. Technol. 2 (2) (2016) 286–291.
[80] Q. Zhi, J.R. Cooperstock, Depth-based image mosaicing for both static and dynamic scenes, in: Proceedings of the International Conference on Pattern Recognition, 2008, pp. 1–4, doi:10.1109/icpr.2008.4761469.
[81] R. Kaur, A. Kaur, R. Mittal, A. Sharma, Fusion enhanced image stitching using Dct and Dchwt, J. Eng. Res. Appl. 8 (6) (2018) 78–83, doi:10.9790/9622-0806017883.
[82] D. Fraser, R.H. Pouliot, Monitoring land cover change and ecological integrity in Canada's National Parks, Remote Sens. Environ. 113 (2009) 1397–1409, doi:10.1016/j.rse.2008.06.019.
[83] A. Vijayakumaran Nair, D. Loganathan, Enhancement in image mosaicing using voronoi and SURF algorithm, IJCSN Int. J. Comput. Sci. Netw. 6 (35) (2017) 313–319.
[84] C. Kallimani, R. Heidarian, F.K. van Evert, B. Rijk, L. Kooistra, UAV-based multispectral & thermal dataset for exploring the diurnal variability, radiometric & geometric accuracy for precision agriculture, Open Data J. Agric. Res. 6 (2017) (2020) 1–7 June, doi:10.18174/odjar.v6i0.16317.
[85] D. Ghosh, N. Kaabouch, W. Semke, Super-resolution mosaicing of unmanned aircraft system (UAS) surveillance video frames, Int. J. Sci. Eng. Res. 4 (2) (2013) 1–9.
[86] P. Krämer, O. Hadar, J. Benois-Pineau, J.P. Domenger, Use of motion information in super-resolution mosaicing, in: Proceedings of the International Conference on Image Processing, ICIP, 2006, pp. 357–360, doi:10.1109/ICIP.2006.313167. October.
[87] E. Adel, M. Elmogy, H. Elbakry, Real time image mosaicing system based on feature extraction techniques, in: Proceedings of the 9th International Conference on Computer Engineering & Systems (ICCES), 2014, pp. 339–345, doi:10.1109/ICCES.2014.7030983.
[88] S. Lovegrove, A.J. Davison, Real-time spherical mosaicing using whole image alignment, in: Proceedings of the 11th European Conference on Computer Vision, 2010, pp. 73–86, doi:10.1007/978-3-642-15558-1_6.
[89] E. Adel, M. Elmogy, H. Elbakry, Image stitching system based on ORB feature-based technique and compensation blending, Int. J. Adv. Comput. Sci. Appl. 6 (9) (2015) 55–62, doi:10.14569/ijacsa.2015.060907.
[90] A. Vedaldi, VLFeat - an open and portable library of computer vision algorithms, Assoc. Comput. Mach. 10 (10) (2010) 1–4 [Online]. Available: https://www.vlfeat.org/applications/sift-mosaic-code.html .
[91] Z. Qu, W. Bu, L. Liu, The algorithm of seamless image mosaic based on A-KAZE features extraction and reducing the inclination of image, IEE J. Trans. Electr. Electron. Eng. 13 (1) (2018) 134–146, doi:10.1002/tee.22507.
[92] V. Li, Z. Isler, Large scale image mosaic construction for agricultural applications, IEEE Robot. Autom. Lett. 1 (1) (2016) 295–302.
[93] R. Unnikrishnan, A. Kelly, Mosaicing large cyclic environments for visual navigation in autonomous vehicles, Proc. IEEE Int. Conf. Robot. Autom. 4 (2002) 4299–4306 May, doi:10.1109/robot.2002.1014434.
[94] S. Michahial, S.U. Asst, Automatic image mosaicing using sift, RANSAC and homography, Certif. Int. J. Eng. Innov. Technol. 9001 (10) (2008) 2277–3754.
[95] T. Yang, J. Li, J. Yu, S. Wang, Y. Zhang, Diverse scene stitching from a large-scale aerial video dataset, Remote Sens. 7 (6) (2015) 6932–6949, doi:10.3390/rs70606932.
[96] P. Nagabhushan, V.E. Jathanna, Mosaicing of text contents from consecutive frames in pedestal shot videos, Int. J. Eng. Res. V4 (07) (2015) 1006–1013, doi:10.17577/ijertv4is070808.
[97] A. Pundhir, S. Gawande, Optimization technique for image mosaicing using local visual descriptor, Int. J. Adv. Eng. Technol. 03 (07) (2016) 45–51 [Online]. Available: www.ijaetmas.com .
[98] M.Z. Bonny, M.S. Uddin, Image stitching algorithm: an optimization between correlation-based and feature-based method, Int. J. Comput. Sci. Inf. Secur. 16 (6) (2018) 150–157.
[99] N. Geng, D. He, Y. Song, Camera image mosaicing based on an optimized SURF algorithm, TELKOMNIKA Indones. J. Electr. Eng. 10 (8) (2012) 2183–2194, doi:10.11591/telkomnika.v10i8.1658.
[100] R. Szeliski, Image mosaicing for tele-reality applications, in: Proceedings of the IEEE Workshop on Applications of Computer Vision, 1994, pp. 44–53, doi:10.1109/acv.1994.341287.
[101] L.H. Zou, D. Zhang, A. Wulamu, Dynamic scene stitching driven by visual cognition model, Sci. World J. 2014 (2014) 1–10, doi:10.1155/2014/981724.
[102] A. Lati, M. Belhocine, N. Achour, Efficient fuzzy based image mosaicing algorithm for overlapped aerial images, in: Proceedings of the 15th International Conference on Informatics in Control, Automation and Robotics, 2, ICINCO, 2018, pp. 229–236, doi:10.5220/0006826702290236.

[103] D. Kaimaris, P. Patias, M. Sifnaiou, UAV and the comparison of image processing software, Int. J. Intell. Unmanned Syst. 5 (1) (2017) 18–27, doi:10.1108/IJIUS-12-2016-0009.
[104] S. Zhou, C. Luo, On mosaicing 3D broken objects based on multiscale Fourier descriptors, in: Proceedings of the 2nd International Conference on Information Science and Engineering, ICISE2010, 2010, pp. 1352–1355, doi:10.1109/ICISE.2010.5688886.
[105] J. König, P. O'Leary, Hyper resolution image mosaics with unbounded vertical field of view, Comput. Ind. 122 (2020) 1–10, doi:10.1016/j.compind.2020.103281.
[106] G.R. Vinod, R. Anita, Implementation of FFT based automatic image mosaicing, Int. J. Adv. Res. Electr. Electron. Instrum. Eng. 2 (12) (2013) 6002–6009.
[107] K. Chaiyasarn, T.K. Kim, F. Viola, R. Cipolla, K. Soga, Image mosaicing via quadric surface estimation with priors for tunnel inspection, in: Proceedings of the International Conference on Image Processing, ICIP,, 2009, pp. 537–540, doi:10.1109/ICIP.2009.5413902.
[108] T. Xiang, G.S. Xia, L. Zhang, Image stitching with perspective-preserving warping, ISPRS Ann. Photogramm. Remote Sens. Spat. Inf. Sci. 3 (2016) 287–294, doi:10.5194/isprs-annals-III-3-287-2016.
[109] S. Shukla, R. Dhir, R. Rani, Digital image mosaicing using optimized KD-tree search, Int. J. Eng. Res. Technol. 3 (8) (2014) 181–183.
[110] J. Chen, Q. Xu, L. Luo, Y. Wang, S. Wang, A robust method for automatic panoramic UAV image mosaic, Sensors 19 (8) (2019) 1–17 (Switzerland), doi:10.3390/s19081898.
[111] Y. Yang, X. Lee, Four-band thermal mosaicking: a new method to process infrared thermal imagery of urban landscapes from UAV flights, Remote Sens. 11 (11) (2019), doi:10.3390/rs11111365.
[112] K.S.V. Prathap, S.A.K. Jilani, P.R. Reddy, A critical review on image mosaicing, in: Proceedings of the International Conference on Computer Communication and Informatics, ICCCI, 2016, pp. 1–8, doi:10.1109/ICCCI.2016.7480028.
[113] V.A. Dilipsinh Bheda, M. Joshi, A study on features extraction techniques for image mosaicing, Int. J. Innov. Res. Comput. Commun. Eng. 2 (3) (2014) 3432–3437.
[114] M. Aghaei, S. Leva, F. Grimaccia, PV power plant inspection by image mosaicing techniques for IR real-time images, in: Proceedings of the IEEE 44th Photovoltaic Specialist Conference, PVSC, 2017, pp. 3462–3467, doi:10.1109/PVSC.2017.8366734.
[115] S. Bu, Y. Zhao, G. Wan, Z. Liu, Map2DFusion: real-time incremental UAV image mosaicing based on monocular SLAM, in: Proceedings of the IEEE International Conference on Intelligent Robots and Systems, 2016, pp. 4564–4571, doi:10.1109/IROS.2016.7759672.
[116] E. Garcia-Fidalgo, A. Ortiz, Fast image mosaicking using incremental bags of binary words, in: Springer Tracts in Advanced Robotics, 122, Springer, 2018, pp. 141–156, doi:10.1007/978-3-319-75993-7_8.
[117] K. Loewke, D. Camarillo, W. Piyawattanametha, D. Breeden, K. Salisbury, Real-time image mosaicing with a hand-held dual-axes confocal microscope, Endosc. Microsc. III 6851 (2008) (2008) 68510F February, doi:10.1117/12.764322.
[118] Z. Hossein-Nejad, M. Nasri, Clustered redundant keypoint elimination method for image mosaicing using a new Gaussian-weighted blending algorithm, Vis. Comput. 38 (2022) 1991–2007, doi:10.1007/s00371-021-02261-9.
[119] J.K. Gomez-Reyes, J.P. Benitez-Rangel, L.A. Morales-Hernadez, E. Resendiz-Ochoa, K.A. Camarillo-Gomez, Image mosaicing applied on UAVs survey, Appl. Sci. 12 (2729) (2022) 1–21, doi:10.3390/app12052729.
[120] K.A. Aruna, et al., Image mosaicing for neonatal fundus images, in: Proceedings of the 8th International Conference on Smart Computing Communications (ICSCC), 2021, pp. 100–105.
[121] Roberto de Lima, Aldrich A. Cabrera-Ponce, Jose Martinez-Carranza, Parallel Hashing-Based Matching for Real-Time Aerial Image Mosaicing, Real Time Image Process. 18 (2021) 143–156.
[122] M.K. Vishwakarma, A. Bhuyan, Image mosaicking using improved auto-sorting algorithm and local difference-based Harris features, Multimed. Tools Appl. 79 (2020) 23599–23616, doi:10.1007/s11042-020-09124-w.